Struct Multidisc Optim (2008) 35:341–363
DOI 10.1007/s00158-007-0137-z

INDUSTRIAL APPLICATION

Surrogate based optimization of helicopter rotor blades for vibration reduction in forward flight

Bryan Glaz · Peretz P. Friedmann · Li Liu

Received: 17 July 2006 / Revised: 6 February 2007 / Accepted: 19 March 2007 / Published online: 23 June 2007

Abstract The effectiveness of surrogate modeling of helicopter vibrations, and the use of the surrogates for minimization of helicopter rotor vibrations are studied. The accuracies of kriging, radial basis function interpolation, and polynomial regression surrogates are compared. In addition, the surrogates are used to generate an objective function which is employed in an optimization study. The design variables consist of the cross-sectional dimensions of the structural member of the blade and non-structural masses. The optimized blade is compared with a baseline rotor blade which resembles an MBB BO-105 blade. Results indicate that: (a) kriging surrogates best approximate vibratory hub loads over the entire design space and (b) the surrogates can be used effectively in helicopter rotor vibration reduction studies.

Keywords Kriging · Surrogate based optimization · Helicopter · Vibration reduction

Nomenclature

c	Blade chord
C_W	Helicopter weight coefficient
C_{d0}	Blade profile drag coefficient
C_{df}	Flat plate drag coefficient
$\mathbf{D}$	Vector of design variables
E	Young's modulus
$f(\mathbf{x})$	Assumed polynomials which account for the 'global' behavior in kriging
F_{4X}, F_{4Y}, F_{4Z}	4/rev hub shears, non-dimensionalized by $m_0\Omega^2 R^2$
$\hat{F}_{4X}$, $\hat{F}_{4Y}$, $\hat{F}_{4Z}$	Surrogates for the non-dimensional 4/rev hub shears
g($\mathbf{D}$)	Contraints
h	Height of the blade cross-section
J	Objective function
$\hat{J}$	Surrogate objective function
J_P	Mass polar moment of inertia of the rotor
m_0	Baseline mass per unit length
m_{ns}	Non-structural mass located at the elastic axis
M_{4X}, M_{4Y}, M_{4Z}	4/rev hub moments, non-dimensionalized by $m_0\Omega^2 R^3$
$\hat{M}_{4X}$, $\hat{M}_{4Y}$, $\hat{M}_{4Z}$	Surrogates for the non-dimensional 4/rev hub moments
N_b	Number of rotor blades
N_c	Number of behavior constraints
N_{dv}	Number of design variables
N_{sp}	Number of sample points
N_{tp}	Number of test points
p_k, ϑ_k	Fitting parameters in kriging corresponding to the k^{th} design variable
R	Blade radius

B. Glaz (✉) · P. P. Friedmann · L. Liu
Department of Aerospace Engineering,
The University of Michigan,
Ann Arbor, MI 48109, USA
e-mail: bglaz@umich.edu

P. P. Friedmann
e-mail: peretzf@umich.edu

L. Liu
e-mail: ryanliu@umich.edu

$\mathrm{R}_{\mathrm{krg}}$	Spatial correlation matrix used in kriging
$R_{\mathrm{krg}}(\cdot)$	Spatial correlation function in kriging
$\mathrm{r}_{krg}(\mathbf{x})$	Spatial correlation vector in kriging
t_1, t_2, t_3	Thicknesses of the blade cross-section, see Fig. 3
$\mathbf{w}$	Vector or coefficients in RBF interpolation, with elements w_i
$\mathbf{x}^{(i)}$	i^{th} sample point
x_1, x_2	Cross-sectional dimensions, see Fig. 3
X_{FA}, Z_{FA}	Longitudinal and vertical offsets between rotor hub and helicopter aerodynamic center, see Fig. 6
X_{FC}, Z_{FC}	Longitudinal and vertical offsets between rotor hub and helicopter center of gravity, see Fig. 6
$y(\mathbf{x})$	Unknown function to be approximated
$y^{(i)}$	output response at $\mathbf{x}^{(i)}$
$\mathbf{y}$	Vector of observed function outputs
$\hat{y}(\mathbf{x})$	Approximation of $y(\mathbf{x})$
$\bar{y}$	Mean of the absolute values of the responses
$Z(\mathbf{x})$	Realization of a stochastic process in kriging
α_d	Flight descent angle, see Fig. 6
β	Constant used in kriging
$\hat{\beta}$	Generalized least squares estimate of β
$\beta_0, \beta_i, \beta_{ij}$	Fitting coefficients in polynomial regression
β_p	Blade precone angle
ϵ_{pr}	Approximation error in polynomial regression
$\varepsilon^{(tp)}, \varepsilon^{(cv)}$	Absolute percent error, based on test points and leave-one-out cross validation
λ_k	Hover stability eigenvalue for k^{th} mode
ζ_k, ω_k	Real and imaginary parts of λ_k, respectively
μ	Advance ratio
υ	Poisson's ratio
Ω	Rotor angular speed
$\omega_{F1}, \omega_{L1}, \omega_{T1}$	Fundamental rotating flap, lead-lag and torsional frequencies, /rev
ω_L, ω_U	Lower and upper bounds for frequency constraints, /rev
$\Phi_{\mathrm{RBF}}(\cdot)$	Spatial correlation function in RBF interpolation
Φ_{RBF}	Spatial correlation matrix in RBF interpolation
$\Phi_{\mathrm{RBF}}(\mathbf{x})$	Spatial correlation vector in RBF interpolation
ρ_{filler}	Material density for non-structural filler mass
ρ_{struct}	Material density for the structural member of the blade
σ	Rotor solidity
$\sigma_{allowable}$	Allowable blade stress
$\sigma_{xx}, \sigma_{x\eta}, \sigma_{x\zeta}$	Blade stresses
σ^2_{var}	Variance of the Gaussian process $Z(\mathrm{x})$
σ_Y,	Yield stress
$\hat{\sigma}^2_{var}$	Generalized least squares estimate of σ^2_{var}
τ	Fitting parameter in RBF interpolation
θ_{pt}	Blade built-in pre-twist angle

1 Introduction

Vibration is one of the most critical concerns in the design of modern rotorcraft. Stricter demands for enhanced performance, comfort, and customer acceptance require designs with reduced vibration levels. In helicopters, the dominant source of vibrations is the rotor, which transfers vibrations to the rotor hub and fuselage at harmonics that are predominantly N_b/rev, where N_b is the number of blades.

During the last 25 years, two principal approaches to vibration reduction have emerged. The first approach is passive and uses structural/multidisciplinary optimization for reducing vibrations (Friedmann 1991; Celi 1999; Ganguli 2004), while the second approach utilizes active control methods (Friedmann and Millott 1995; Patt et al 2005). This paper focuses on the passive approach. In the passive approach the vibration reduction problem is formulated as a mathematical optimization problem subject to appropriate constraints. The objective function consists of a suitable combination of the N_b/rev hub shears and moments that are computed from an aeroelastic response code; the constraints are blade stability margins, frequency constraints, an autorotation constraint, constraints associated with the blade geometry, and a constraint on the blade stresses. The design variables can be dimensions of the blade cross-section, mass and stiffness distributions along the span, or geometrical parameters which define advance geometry tips. Typical levels of vibration reduction achieved with passive approaches have been in the range of 30-60%.

Due to the complex rotary-wing aerodynamic environment, the aeroelastic response simulations needed for vibratory load calculations are computationally expensive. Therefore numerous evaluations of the vibration objective function are costly. Consequently, direct combination of the objective function generated by the aeroelastic response simulation with traditional optimization algorithms is computationally very

expensive. Moreover, traditional optimization search algorithms can converge to local optima, which are known to occur in this class of problems.

To overcome these obstacles, approximation concepts have been used. A widely used approach for approximating the vibration objective function and constraints is to use Taylor series expansions about local design points (Schmit and Miura 1976). The derivatives needed for the Taylor series are calculated using difference formulas, or analytical sensitivity derivatives. These approximations of the objective function and constraints are used to replace the actual problem with an approximate one that is used in conjunction with an optimizer to obtain an optimal design. Representative examples of the application of this method to the rotor vibration reduction problem can be found in Yuan and Friedmann (1998) and Yuan and Friedmann (1995), in which vibration reduction of composite rotor blades with advanced geometry tips in forward flight was studied. The disadvantages of this method are that it utilizes a local approximation in the vicinity of a design point and a local search procedure. Even when augmenting such methods with move limits or a trust region strategy (Wujek and Renaud 1998; Alexandrov et al 1998), convergence is only guaranteed to a local optimum.

An alternative to the local Taylor expansion method is to use global approximation methods (Queipo et al 2005); i.e. methods which try to capture the behavior of a function over the entire design space. The advantages of surrogate-based optimization (SBO) with global approximations are threefold: fewer "true" function evaluations (thus fewer expensive aeroelastic simulations), the formulation is conducive to parallel computing, and facilitation of a more "global" search of the design space. In one SBO application, Ganguli (2002) used a 2^{nd} order polynomial global approximation of the vibration objective function and obtained 30% vibration reduction. The 2^{nd} order polynomial was found to be accurate only in the vicinity of the baseline design. In addition to polynomials, there is a class of global approximation methods based on stochastic processes, which can be used in a global search of the design space (Won and Ray 2005). Illustrative examples of the benefits of SBO with stochastic process based approximations can be found in the studies by Sóbester et al (2004) and Booker et al (1999).

In Sóbester et al (2004), surrogate based methods and conventional methods – i.e. no approximations of the objective function combined with genetic algorithms and gradient based search methods – were used to find the optima of closed form five-dimensional test functions. The test functions were not computationally expensive to evaluate, and were only used to test the SBO method. In addition, Sóbester et al (2004) took advantage of the opportunities for parallel computing afforded by SBO. Not only did SBO converge to the optima in less time, but the optimum yielded by SBO was superior to the optimum obtained from conventional optimization algorithms which do not use approximations of the objective function. Sóbester et al (2004) employed a stochastic process based approximation method known as radial basis function (RBF) interpolation.

In Booker et al (1999), surrogate based methods were applied to minimization of helicopter vibration, using 31 design variables to characterize the rotor blade. The cross-sectional design variables were mass, center of gravity offset from the elastic axis, and the blade stiffnesses. The analysis code Tech01 (Shultz et al 1994) was used to generate hub shears and moments, and the stochastic process based method known as kriging interpolation was used to approximate the objective function. The results showed that kriging could be used to find reduced vibration designs in an efficient manner. However, it is important to note that the principal focus of Booker et al (1999) was on the effectiveness of surrogate objective functions, and therefore accurate modeling of the aerodynamic environment of a rotor blade during flight was not considered to be important. Consequently, accurate free wake models were sacrificed for a computationally less expensive prescribed wake model. Furthermore, no constraints were placed on the aeroelastic stability of the blade. Thus, the model of the helicopter vibratory loads was not sufficiently reliable to produce a realistic blade design.

It is important to note that various global approximation methods have been compared for different engineering problems (Chen et al 2006; Simpson et al 2004, 2001b), and there is no universal conclusion as to which method is best. For instance, some studies have found that polynomials perform as well or better than other approximation methods, while others have concluded that RBF interpolation or kriging are the best methods (Simpson et al 2001a; Stander et al 2004; Jin et al 2001; Forsberg and Nilsson 2005; Palmer and Realff 2002a,b). Thus, a single approximation method has not distinguished itself as the most suitable for engineering applications.

An important feature of the surrogate based optimization approach using interpolation is that the method is computationally effective when the number of design variables is relatively small (less than 50). This is compatible with helicopter rotor blade optimization problems where the number of important design variables can be limited to this range. The overall objective

of this paper is to examine the applicability of global approximation methods to the rotor blade vibration reduction problem in forward flight. To achieve this objective, the suitability of three approximation methods commonly used in optimization applications are considered:

1. Polynomial Regression
2. Radial Basis Functions (RBF's)
3. Kriging

2 Overview of the aeroelastic response and stability analysis

The simulation code used in this study is based on a comprehensive aeroelastic analysis code (Millott and Friedmann 1994; Yuan and Friedmann 1995; Myrtle and Friedmann 2001; de Terlizzi and Friedmann 1999; Depailler and Friedmann 2002; Patt et al 2006; Liu et al 2005). The aeroelastic response analysis can represent the behavior of hingeless rotor blades as shown in Fig. 1, with actively controlled flaps; as well as blades with advanced geometry tips as shown in Fig. 2. The key ingredients of the aeroelastic response analysis are: (1) the structural dynamic model, (2) the unsteady aerodynamic model and (3) a coupled trim/aeroelastic response procedure that is required for the computation of the steady state blade response. The aeroelastic response analysis and overviews of the blade stress calculations and aeroelastic stability in hover analysis are described next.

2.1 Structural dynamic model

The structural dynamic model is based on an analysis developed by Yuan and Friedmann (1995, 1998) which is capable of modeling composite blades with transverse shear deformations, cross-sectional warping,

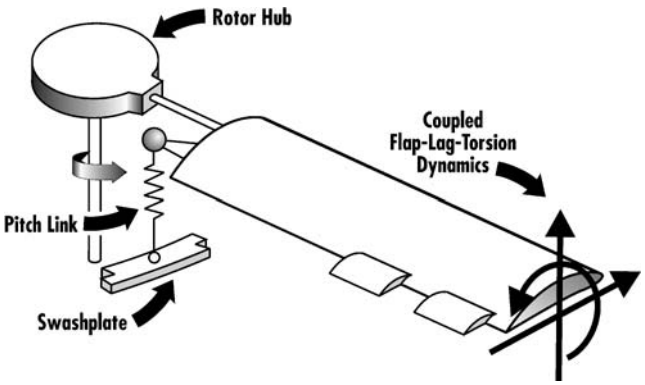

Fig. 1 Helicopter rotor blade with trailing edge flaps

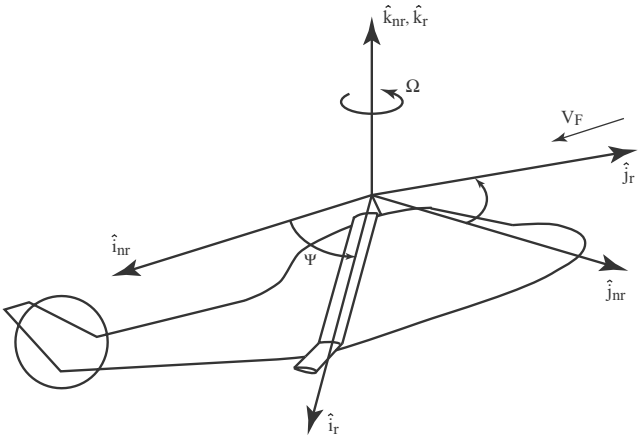

Fig. 2 A blade with advanced geometry tip

and swept tips. This study is limited to the behavior of isotropic blades with spanwise varying properties. The equations of motion are formulated using a finite element discretization of Hamilton's principle, with the assumption that the blade undergoes moderate deflections. The beam type finite elements used for the discretization have 23 nodal degrees of freedom. Normal modes are used to reduce the number of structural degrees of freedom. In this study, eight modes are used: the first 3 flap modes, first 2 lead-lag modes, first 2 torsional modes, and the first axial mode.

2.2 Aerodynamic model

The attached flow blade section aerodynamics are calculated using a rational function approach (RFA) (Myrtle and Friedmann 2001; Myrtle 1998). The RFA approach is a two-dimensional unsteady time-domain theory that accounts for compressibility as well as variations in the oncoming flow velocity. This two-dimensional aerodynamic model is linked to an enhanced free-wake model which provides a non-uniform inflow distribution at closely spaced azimuthal steps (Patt et al 2005; Johnson 1988a,b). Although the simulation code can also account for dynamic stall at high advance ratios (Depailler and Friedmann 2002), dynamic stall was not considered in this paper because the vibration levels being approximated are those due to blade vortex interaction (BVI), which occurs at low advance ratios.

2.3 Coupled trim/aeroelastic response

The combined structural and aerodynamic equations form a system of coupled ordinary differential equations that are cast into first order state variable form (Myrtle and Friedmann 2001) and integrated in the

time domain using the Adams-Bashforth predictor-corrector algorithm. A propulsive trim procedure, where six equilibrium equations (three forces and three moments) are enforced, is used in this study (Millott and Friedmann 1994; de Terlizzi and Friedmann 1998). The trim equations are solved in a coupled manner with the aeroelastic equations of motion. The vibratory hub shears and moments are found by integrating the distributed inertial and aerodynamic loads over the entire blade span in the rotating frame, then transforming these loads to the hub-fixed non-rotating system, and summing the contributions from each blade (Yuan and Friedmann 1995). In the process, cancellation of various terms occurs and the primary components of the hub shears and moments have a frequency of N_b/rev, which is known as the blade passage frequency.

2.4 Blade stresses

After the blade responses are obtained from the coupled trim/aeroelastic response solution, the stresses in the blade at any spanwise location can be recovered by using strain-displacement and constitutive relations. Solving for the stresses in this manner accounts for the complicated loading a blade encounters and is consistent with the structural dynamic model. The procedure for calculating stresses is as follows:

1. For a given azimuth angle, the displacements at any spanwise location are calculated by the aeroelastic response code.
2. The displacements are then substituted into the nonlinear strain-displacement relations (Yuan and Friedmann 1995), giving the strains at any spanwise location.
3. Stresses are calculated from the stress-strain relations.

This calculation gives the blade stresses at any spanwise location and at any azimuth angle.

2.5 Aeroelastic stability in Hover

The process for determining the hover stability of the blade is based on the method used by Yuan and Friedmann (1995), and is described below:

1. The non-linear static equilibrium solution of the blade is found for a given pitch setting and uniform inflow, by solving a set of nonlinear algebraic equations. Note that uniform inflow is used only in the hover stability calculation. The forward flight analysis employs a free-wake model for inflow calculation.
2. The governing system of ordinary differential equations are linearized about the static equilibrium solution by writing perturbation equations and neglecting second-order and higher terms in the perturbed quantities. The linearized equations are rewritten in first-order state variable form.
3. The real parts of the eigenvalues of the first-order state variable matrix, $\lambda_k = \zeta_k + i\omega_k$, determine the stability of the system. If $\zeta_k \leq 0$ for all k, the system is stable.

For this study, the linearization process in Yuan and Friedmann (1995) is modified to account for the aerodynamic states introduced by the RFA model. Details of the linearization process with RFA aerodynamics are provided in Appendix A.

3 Formulation of the blade optimization problem

The formulation of the blade optimization problem in forward flight consists of several ingredients: the objective function, design variables, and constraints. The mathematical formulation of the optimization is stated as: Find the vector of design variables **D** which minimizes the *objective function*, i.e. $J(\mathbf{D}) \rightarrow \min$, where the objective function consists of a combination of the N_b/rev oscillatory hub shears and moments. For a four bladed rotor, the objective function is given by

$$J = K_S\sqrt{(F_{4X})^2 + (F_{4Y})^2 + (F_{4Z})^2} + K_M\sqrt{(M_{4X})^2 + (M_{4Y})^2 + (M_{4Z})^2} \quad (1)$$

where K_S and K_M are appropriately selected weighting factors.

The vector of *design variables* **D** consists of the thicknesses t_1, t_2, t_3, and the non-structural mass m_{ns} located at the shear center, which are specified

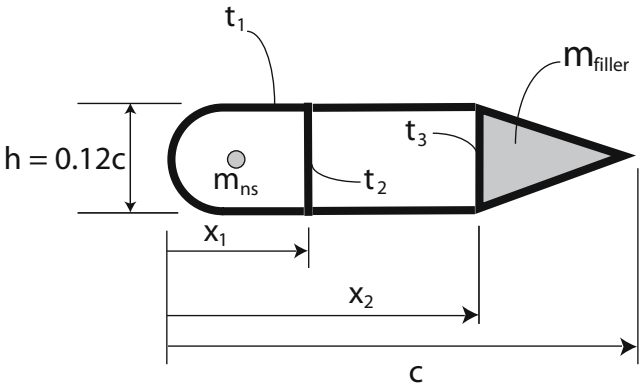

Fig. 3 Simplified model of the blade structural member

at several spanwise locations and shown in Fig. 3. The three thickness design variables were defined at the 0%, 25%, 50%, 75%, and 100% stations, while the non-structural mass design variable was defined at the 68% and 100% blade stations, resulting in a total of 17 design variables. These two blade stations were chosen for the non-structural mass because previous studies have shown that non-structural masses are most effective for vibration reduction when they are distributed over the outboard 1/3 of the blade (Friedmann and Shanthakumaran 1984; Lim and Chopra 1989). The cross-sectional variables were assumed to vary linearly between stations. The non-structural mass at the elastic axis inboard of the 68% station was set to zero. The design variables have *side constraints* to prevent them from reaching impractical values; these are stated as

$$\mathbf{D}_j^{(L)} \le \mathbf{D} \le \mathbf{D}_j^{(U)}, \qquad j = 1, 2, \ldots, N_{dv}. \tag{2}$$

In addition, four types of *behavior constraints*, given by

$$g_i(\mathbf{D}) \le 0, \qquad i = 1, 2, \ldots, N_c, \tag{3}$$

are placed on the design variables. The first type of behavior constraints are *frequency placement constraints*, which are prescribed upper and lower bounds on the fundamental flap, lag, and torsional frequencies of the blade. The frequency placement constraints on the fundamental flap frequency are written as

$$g_{\text{flap}}(\mathbf{D}) = \frac{\omega_{F1}}{\omega_U} - 1 \le 0 \tag{4}$$

and

$$g_{\text{flap}}(\mathbf{D}) = 1 - \frac{\omega_{F1}}{\omega_L} \le 0 \tag{5}$$

where ω_U and ω_L are the prescribed upper and lower bounds on the fundamental flap frequency. Similar constraints are placed on the lag and torsional frequencies, i.e. g_{lag} and g_{torsion}. In addition, all blade frequencies must differ from integer multiples of the angular velocity – 1/rev, 2/rev, 3/rev, …, etc. – to avoid undesirable resonances.

Another behavior constraint is an *autorotational constraint*, which ensures that mass redistributions produced during the optimization do not degrade the autorotational properties of the rotor. Although there are several indices which can be used to represent the autorotational properties of the blade, the one used in this study is to require that the mass polar moment of inertia of the rotor be at least 90% of its baseline value (Celi and Friedmann 1990). Mathematically, this is expressed as

$$g(\mathbf{D}) = 1 - \frac{J_P}{0.9 J_{P0}} \le 0 \tag{6}$$

where J_P is the mass polar moment of inertia of the rotor when it is spinning about the shaft, and J_{P0} is the baseline value.

The third type of behavior constraints are *aeroelastic stability margin constraints*, expressed mathematically as

$$g_k(\mathbf{D}) = \zeta_k + (\zeta_k)_{\min} \le 0, \qquad k = 1, 2, \ldots, N_m \tag{7}$$

where N_m is the number of normal modes, ζ_k is the real part of the hover eigenvalue for the k^{th} mode, and $(\zeta_k)_{\min}$ is the minimum acceptable damping level for the k_{th} mode. It should be noted that the most critical modes for stability are usually the first and second lag modes.

The final behavior constraint is a *yielding constraint* obtained by substituting the blade stresses into Von Mises' criterion, which is expressed mathematically as

$$\frac{2\sigma_{xx}^2 + 6\left(\sigma_{x\eta}^2 + \sigma_{x\zeta}^2\right)}{6} - \frac{\sigma_{allowable}^2}{3} \le 0 \tag{8}$$

where σ_{xx}, $\sigma_{x\eta}$, and $\sigma_{x\zeta}$ are the axial and shear stresses, and $\sigma_{allowable}$ is the material yielding stress divided by a factor of safety. At discrete values of the azimuth angle, (8) is evaluated at spanwise locations corresponding to the finite element nodes. The maximum evaluation of (8) is used for the constraint, and is given as

$$g(\mathbf{D}) = \text{MAX}\left[\frac{2\sigma_{xx}^2 + 6\left(\sigma_{x\eta}^2 + \sigma_{x\zeta}^2\right)}{6} - \frac{\sigma_{allowable}^2}{3}\right] \le 0 \tag{9}$$

where MAX[ ] denotes the maximum value of (8) over each set of azimuth angle and blade stations at which it is evaluated. Therefore the yielding constraint is enforced at the blade station and azimuth angle where the stress condition is most critical.

4 Global approximation methods

The goal in using global approximation, or surrogate, methods is to replace the "true" objective function and expensive constraints with smooth functional relationships of acceptable accuracy that can be evaluated quickly. In order to construct the surrogates, the objective function and constraints must first be evaluated over a set of design points. The surrogate is then generated by fitting the initial design points. Although function evaluations, which come from the expensive helicopter simulations, are needed to form the approximation, this initial investment of computer time is significantly less compared to global searches

using non-surrogate based optimization methods. Once the surrogates have been obtained, they are used to replace the more expensive "true" objective function and constraints in the search for the optimum.

In order to determine the best approach for generating the surrogate objective function, two schemes will be compared: (a) the vibratory hub shears and moments in (1) will be replaced by surrogates and used to build the surrogate objective function, as in (10), and (b) the overall output, J, will be approximated directly. Therefore, 6 responses need to be approximated in the first approach, and 1 response needs to be approximated in the second approach.

$$\hat{J} = K_S\sqrt{(\hat{F}_{4X})^2 + (\hat{F}_{4Y})^2 + (\hat{F}_{4Z})^2} + K_M\sqrt{(\hat{M}_{4X})^2 + (\hat{M}_{4Y})^2 + (\hat{M}_{4Z})^2}. \quad (10)$$

The yielding constraint is the only constraint which requires a forward flight simulation, and is therefore the only computationally expensive constraint. Consequently, a surrogate constraint is used in place of (9) during optimization. Descriptions of several methods for constructing the global approximations are given below.

4.1 Design of computer experiments

When the initial data set is produced by a deterministic computer code (as is the case in the vibration reduction problem), the term "design of computer experiments," is more appropriate than design of experiments (Sacks et al 1989; Simpson et al 2004). The distinction is necessary because in physical experiments there is measurement error and other random sources of noise that cannot be controlled, which affect the choice of the design point. However, in computer experiments, there is no random error; i.e., for a deterministic computer code, a given input will always yield the same output. Thus, the design of computer experiments need only be *space-filling*. Figure 4 illustrates the difference between a conventional design of experiment and a space-filling design. In the figure, locations of design points where experiments are to be conducted, which in this case represent design points where aeroelastic response simulations are performed, are shown for a design space which has two design variables.

A commonly used space-filling design is Latin hypercube sampling (LHS) (McKay et al 1979). In LHS, each design variable is partitioned into N_{sp} equally spaced sections, or strata. Every design variable D_i, where $i = 1, 2, \ldots, N_{dv}$, is sampled once in each strata, which forms N_{dv} vectors of size N_{sp}. The components of the N_{dv} vectors are then randomly combined to form an $N_{sp} \times N_{dv}$ matrix known as a Latin hypercube, where each row corresponds to a design point at which a computer experiment is performed. A major disadvantage of Latin hypercube sampling is that design points can cluster together due to the random process by which design points are created. To prevent this, optimal Latin hypercube (OLH) (Queipo et al 2005) sampling is used in this study to ensure a more uniform (or space-filling) design of computer experiment. Optimal Latin hypercube sampling creates a more uniform design than conventional LHS by maximizing a spreading criteria, rather than randomly creating design points from the samples. Figure 5 illustrates the difference between a conventional Latin hypercube and an optimal Latin hypercube. In this study, the OLH algorithm from the iSIGHT software package is used (Jin et al 2005; Koch et al 2002). Methods for fitting the data points in the OLH are described next.

4.2 Polynomial regression

Suppose a deterministic function of N_{dv} design variables, that needs to be approximated, has been

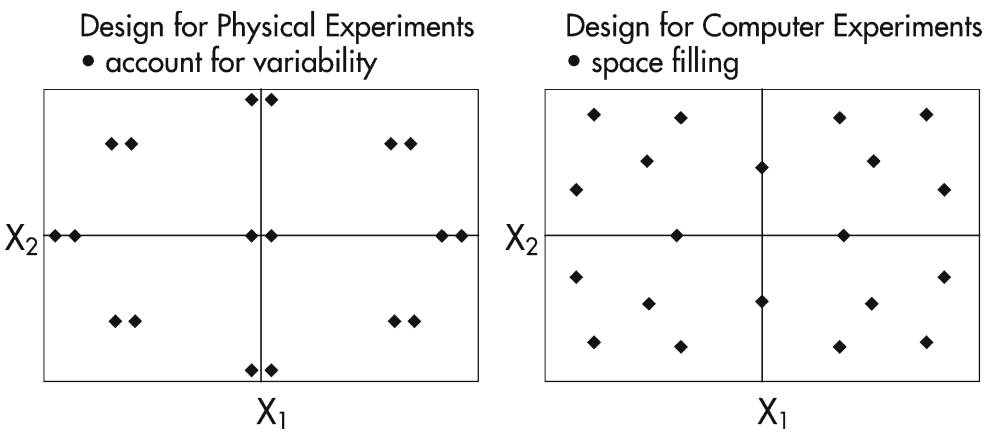

Fig. 4 Design of physical experiment vs. design of computer experiment

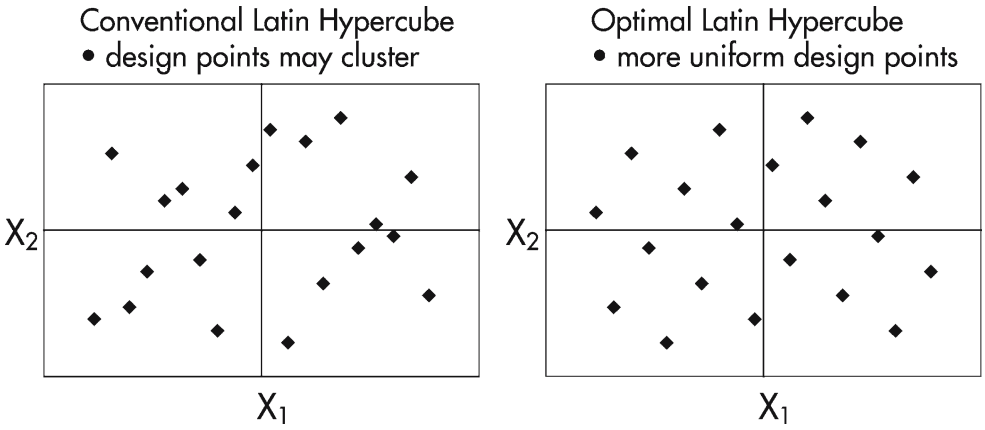

Fig. 5 Conventional LH vs. Optimal LH in two dimensional design space

evaluated at N_{sp} sample points. Sample point i is denoted $\mathbf{x}^{(i)} = (x_1^{(i)}, \ldots, x_{N_{dv}}^{(i)})$ and the associated response is given by $y^{(i)} = y(\mathbf{x}^{(i)})$ for $i = 1, \ldots, N_{sp}$. A polynomial regression approximation to $y(\mathbf{x})$ can be written as

$$y(\mathbf{x}) = \hat{y}(\mathbf{x}) + \epsilon_{\text{pr}} \tag{11}$$

where $\hat{y}(\mathbf{x})$ is the function chosen to approximate the true response $y(\mathbf{x})$, and ϵ_{pr} is the error associated with the approximation. It is important to note that the errors are assumed to be independent; i.e. the errors at two points close together will not necessarily be close. This assumption will be revisited when considering kriging. In this study, 2nd order polynomials are used for $\hat{y}(\mathbf{x})$. The least squares regression approximation is given as (Jin et al 2001)

$$\hat{y}_{pr} = \beta_0 + \sum_{i=1}^{N_{dv}} \beta_i x_i + \sum_{i=1}^{N_{dv}} \sum_{j=1, i<j}^{N_{dv}} \beta_{ij} x_i x_j + \sum_{i=1}^{N_{dv}} \beta_{ii} x_i^2. \tag{12}$$

4.3 Kriging

Kriging is based on the fundamental assumption that errors are correlated, which is in contrast to the assumption of independent or uncorrelated errors made in polynomial regression. This implies that one assumes the errors at two points close together will be close. In fact, the assumption that the errors are uncorrelated is only appropriate when the sources of error are random, such as in the case of measurement error or noise. In the case of deterministic computer simulations, there is no source of random error. Therefore, it is more reasonable to assume that the error terms will be correlated and that this correlation is higher the closer two points are to each other. In kriging, the unknown function $y(\mathbf{x})$ is assumed to be of the form

$$y(\mathbf{x}) = f(\mathbf{x}) + Z(\mathbf{x}) \tag{13}$$

where $f(\mathbf{x})$ is an assumed function (usually polynomial form) and $Z(\mathbf{x})$ is a realization of a stochastic (random) process which is assumed to be a Gaussian process with zero mean and variance of σ_{var}^2, i.e. $Z(\mathbf{x})$ follows a normal, or Gaussian, distribution (Jones et al 1998; Sasena 2002). The function $f(\mathbf{x})$ can be thought of as a global approximation of $y(\mathbf{x})$, while $Z(\mathbf{x})$ accounts for local deviations which ensure that the kriging model interpolates the data points exactly. The covariance matrix of $Z(\mathbf{x})$, which is a measure of how strongly correlated two points are, is given by

$$\text{Cov}[Z(\mathbf{x}^{(i)}), Z(\mathbf{x}^{(j)})] = \sigma_{var}^2 \mathbf{R}_{\text{krg}} \tag{14}$$

where each element of the $N_{sp} \times N_{sp}$ correlation matrix $\mathbf{R}_{\text{krg}}$ is given by

$$(R_{\text{krg}})_{ij} = R_{\text{krg}}(\mathbf{x}^{(i)}, \mathbf{x}^{(j)}) \tag{15}$$

and $R_{\text{krg}}(\mathbf{x}_i, \mathbf{x}_j)$ is a correlation function which accounts for the effect of each interpolation point on every other interpolation point. This function is called the spatial correlation function (SCF) and is chosen by the user. The most commonly used SCF is the Gaussian correlation function,

$$R_{\text{krg}}(\mathbf{x}^{(i)}, \mathbf{x}^{(j)}) = \exp\left[-\sum_{k=1}^{N_{dv}} \vartheta_k |x_k{}^{(i)} - x_k{}^{(j)}|^{p_k} \right], \tag{16}$$

which is also employed in this study. The Gaussian SCF is dependent on the distance between two points. As two points move closer to each other, $|x_k{}^{(i)} - x_k{}^{(j)}| \to 0$, and (16) approaches unity which is the maximum value of the Gaussian SCF. In other words, the Gaussian SCF recovers the intuitive property that the closer two points are to each other, the greater the correlation between the points.

The fitting parameters ϑ_k and p_k are unknown correlation parameters which need to be determined. In order to determine these parameters, the form of $f(\mathbf{x})$ needs to chosen. The most common choice for $f(\mathbf{x})$ is

$f(\mathbf{x}) = \beta$ where β is a constant. Previous studies have found that modeling with the SCF is so effective, that using a constant for the global behavior results in little loss of fidelity (Sasena 2002; Sacks et al 1989; Simpson et al 2001b; Jones et al 1998). Another common simplification, is to fix all $p_k = 2$. When this simplification is combined with the constant global approximation, the approximation method is known as *ordinary kriging*. In the present study, kriging models where p_k are not fixed at 2 will be compared with ordinary kriging models. In order to find ϑ_k and p_k, the generalized least square estimates of β and σ^2_{var}, denoted by $\hat{\beta}$ and $\hat{\sigma}^2_{var}$ respectively, are employed (Sasena 2002; Jones et al 1998):

$$\hat{\beta} = (\mathbf{1}^{\mathrm{T}}(\mathbf{R}_{\mathrm{krg}})^{-1}\mathbf{1})^{-1}\mathbf{1}^{\mathrm{T}}(\mathbf{R}_{\mathrm{krg}})^{-1}\mathbf{y} \tag{17}$$

and

$$\hat{\sigma}^2_{var} = \frac{(\mathbf{y} - \mathbf{1}\hat{\beta})^{\mathrm{T}}(\mathbf{R}_{\mathrm{krg}})^{-1}(\mathbf{y} - \mathbf{1}\hat{\beta})}{N_{sp}} \tag{18}$$

where $\mathbf{1}$ is a vector populated by ones and $\mathbf{y}$ is a vector of observed function outputs at the interpolation points; both vectors are of length N_{sp}. With $\hat{\sigma}^2_{var}$ and $\hat{\beta}$ known, ϑ_k and p_k are found such that a likelihood function (Schonlau 1997; Sasena 2002; Jones et al 1998) is maximized. The likelihood function, given in (19), is a measure of the probability of the sample data being drawn from a probability density function associated with a Gaussian process. Since the stochastic process associated with kriging has been assumed to be a Gaussian process, one seeks the set of ϑ_k and p_k that maximize the probability that the interpolation points have been drawn from a Gaussian process.

$$-\frac{\left[N_{sp}\ln(\hat{\sigma}^2_{var}) + \ln|\mathbf{R}_{\mathrm{krg}}|\right]}{2} \tag{19}$$

The maximum likelihood estimates (MLE's) of ϑ_k and p_k represent the "best guesses" of the fitting parameters. Any values of ϑ_k and p_k would result in a surrogate which interpolates the sample points exactly, but the "best" kriging surrogate is found by optimizing the likelihood function. This auxiliary optimization process can result in significant fitting time depending on the size of the system. Due to the optimization process needed to create the kriging surrogate, kriging is only appropriate when the time needed to generate the interpolation points is much larger than the time to interpolate the data – which is the case in the helicopter vibration problem. With all parameters known, the kriging approximation to a function $y(\mathbf{x})$ can be written as (Sasena 2002; Simpson et al 2001b; Sacks et al 1989; Jones et al 1998)

$$\hat{y}_{\mathrm{krg}} = \hat{\beta} + \mathbf{r}_{\mathrm{krg}}(\mathbf{x})^{\mathrm{T}}(\mathbf{R}_{\mathrm{krg}})^{-1}(\mathbf{y} - \mathbf{1}\hat{\beta}) \tag{20}$$

where

$$\mathbf{r}_{\mathrm{krg}}(\mathbf{x}) = \left[R_{\mathrm{krg}}(\mathbf{x}, \mathbf{x}^{(1)}), R_{\mathrm{krg}}(\mathbf{x}, \mathbf{x}^{(2)}), \ldots, R_{\mathrm{krg}}(\mathbf{x}, \mathbf{x}^{(N_{sp})})\right]^{\mathrm{T}} \tag{21}$$

The column vector $\mathbf{r}_{\mathrm{krg}}(\mathbf{x})$ of length N_{sp} is the correlation vector between an arbitrary point $\mathbf{x}$ and the interpolation points, $\mathbf{x}^{(1)}, \ldots, \mathbf{x}^{(N_{sp})}$.

4.4 Radial basis function overview

Radial basis function (RBF) interpolation is similar to kriging in the sense that they are based on Gaussian correlation functions. However, in this paper RBF interpolation refers to an approximation method based on Gaussian correlation functions that does not include a constant global approximation term, unlike kriging. The method of RBF interpolation used in this study is based on the method employed in Sóbester et al (2004). A brief description of the methodology for generating the RBF surrogate is described next.

In RBF surrogates, the approximate response is a weighted sum of basis functions:

$$\hat{y} = \sum_{i=1}^{N_{sp}} w_i \phi_{\mathrm{RBF}}\left(\left\|\mathbf{x} - \mathbf{x}^{(i)}\right\|\right) \tag{22}$$

where $\phi_{\mathrm{RBF}}(*)$ is typically a non-linear function depending on the Euclidean distance (denoted by $\left\|\mathbf{x} - \mathbf{x}^{(i)}\right\|$) between two design points. The coefficients, w_i, must be found such that the surrogate interpolates the initial data points. Thus, the following condition must be satisfied for $j = 1, \ldots, N_{sp}$:

$$y\left(\mathbf{x}^{(j)}\right) = \sum_{i=1}^{N_{sp}} w_i \phi_{\mathrm{RBF}}\left(\left\|\mathbf{x}^{(j)} - \mathbf{x}^{(i)}\right\|\right) \tag{23}$$

By defining the vectors $\mathbf{w} = [w_1, w_2, \ldots, w_{N_{sp}}]^{\mathrm{T}}$, $\mathbf{y} = [y_1, y_2, \ldots, y_{N_{sp}}]$, and the $N_{sp} \times N_{sp}$ spatial correlation matrix Φ_{RBF} with elements $(\Phi_{\mathrm{RBF}})_{ij} = \phi_{\mathrm{RBF}}\left(|\mathbf{x}^{(i)} - \mathbf{x}^{(j)}|\right)$, (23) can be rewritten as

$$\Phi_{\mathrm{RBF}}\mathbf{w} = \mathbf{y}^{\mathrm{T}} \tag{24}$$

If the inverse of Φ_{RBF} exists, then the weighting coefficients are

$$\mathbf{w} = (\Phi_{\mathrm{RBF}})^{-1}\mathbf{y}^{\mathrm{T}} \tag{25}$$

and the RBF surrogate is

$$\hat{y}_{RBF}(\mathbf{x}) = \boldsymbol{\phi}_{\mathrm{RBF}}\mathbf{w} = \boldsymbol{\phi}_{\mathrm{RBF}}(\Phi_{\mathrm{RBF}})^{-1}\mathbf{y}^{\mathrm{T}} \tag{26}$$

where

$$\boldsymbol{\phi}_{\mathrm{RBF}} = \left[\phi_{\mathrm{RBF}}\left(\left\|\mathbf{x}-\mathbf{x}^{(1)}\right\|\right), \ldots, \phi_{\mathrm{RBF}}\left(\left\|\mathbf{x}-\mathbf{x}^{(N_{sp})}\right\|\right)\right]. \tag{27}$$

As stated above, (26) shows that the RBF surrogate does not include a constant global approximation term, unlike (20) which includes $\hat{\beta}$. Gaussian correlation functions of the form given by (28) are used for the basis functions in (22).

$$\phi_{\mathrm{RBF}}(\eta) = \exp(-\eta^2/2\tau^2) \tag{28}$$

In this case, the dummy variable η would be $\left\|\mathbf{x}-\mathbf{x}^{(i)}\right\|$. As described in Sóbester et al (2004), the fitting parameter τ is found by *leave-one-out cross validation*. This process is described below:

1. The design variables are scaled to vary from 0 to 1. The possible values of τ are then spread over the domain $[10^{-1}, 10^{1}]$ on a logarithmic scale. This domain was used because the spatial correlation matrix did not become ill-conditioned during the fitting process with these bounds on τ.
2. For each value of τ, N_{sp} RBF models are created, leaving one interpolation point out each time, as if only $(N_{sp}-1)$ interpolation points exist. Therefore, for each value of τ, N_{sp} evaluations of (26) are required and each evaluation involves the inversion of the $N_{sp} \times N_{sp}$ matrix Φ_{RBF}. Since a large set of τ can lead to an excessive number of evaluations of (26), only 15 values for τ were considered so that the RBF remains computationally tractable.
3. The difference between the true response at the left out point and the response predicted at the left out point by the RBF model based on $(N_{sp}-1)$ points is computed.
4. The value of τ that minimizes the sum of these residuals is selected as the fitting parameter.

5 Results

This section presents accuracy and robustness measures of the approximation methods that have been described, as well as vibration reduction results using surrogate objective functions. The helicopter configuration used in all computations is given in Table 1. The simulations are conducted at an advance ratio of 0.15 and descent angle of 6.5°, where high vibration levels due to strong blade vortex interaction (BVI) are encountered (Patt et al 2006). Figure 6 illustrates a helicopter in descent; this figure is also employed for the propulsive trim calculation.

Table 1 Rotor and helicopter parameters needed for the computations

Dimensional Data	
$R = 4.91\,\mathrm{m}$	$\Omega = 425$ RPM
Non-Dimensional Data	
$N_b = 4$	$c = 0.05498R$
$\beta_p = 0.0°$	$C_{do} = 0.01$
$\theta_{\mathrm{pt}} = 0°$	$\alpha_{\mathrm{d}} = 6.5°$
$\mu = 0.15$	$C_W = 0.005$
$\sigma = 0.07$	$C_{df} = 0.01$
$X_{FA} = 0.0$	$Z_{FA} = 0.3$
$X_{FC} = 0.0$	$Z_{FC} = 0.3$

In addition to the information provided in Table 1, additional information is needed for the fixed cross sectional parameters, objective function, constraints, and the finite element discretization of the blade. The material properties and the chordwise locations of the vertical walls are given in Table 2. Details on how x_1 and x_2 were determined can be found in Glaz et al (2006).

The weighting factors in the objective function, K_S and K_M, are selected to be 1. These weighting factors result in an objective function which represents the sum of the 4/rev oscillatory hub shear resultant and the 4/rev oscillatory hub moment resultant in the hub-fixed non-rotating frame. For this study, the following side constraints are enforced:

$$1.0\,\mathrm{mm} \le t_1 \le 8.0\,\mathrm{mm} \tag{29}$$

$$1.0\,\mathrm{mm} \le t_2, t_3 \le 12.0\,\mathrm{mm} \tag{30}$$

$$0.0 \le m_{ns}/m_0 \le 0.25 \tag{31}$$

The upper and lower bounds used for the frequency placement constraints are given in Table 3, and are similar to those used in Lim and Chopra (1991), which also used cross-sectional dimensions as design variables.

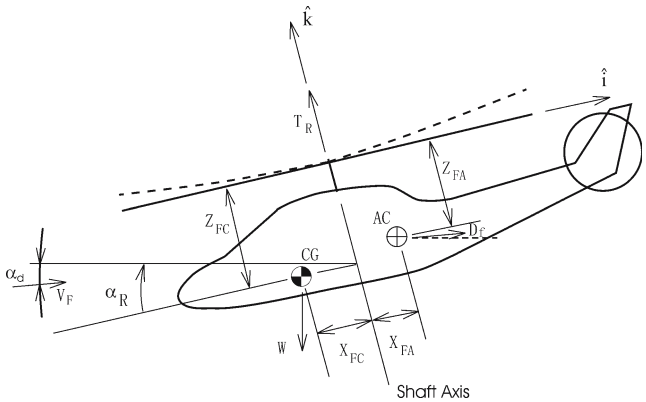

Fig. 6 Helicopter in descent flight condition

Table 2 Fixed parameters defining the structure and cross section

Aluminum Material Properties	
$E = 70.7\,\text{GPa}$	
$\nu = 0.33$	
$\rho_{\text{struct}} = 2700\,\text{kg/m}^3$	
$\sigma_Y = 324\,\text{MPa}$	
Non-structural Filler Mass Density	
$\rho_{\text{filler}} = 237.4\,\text{kg/m}^3$	
Locations of the Vertical Walls	
$x_1 = 65.4\,\text{mm}$	$x_2 = 111.6\,\text{mm}$

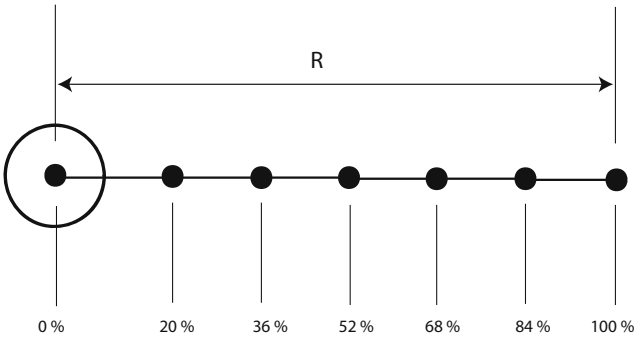

Fig. 7 Finite element node locations

In the aeroelastic stability constraints given by (7), the minimum acceptable damping for all modes, $(\zeta_k)_{\min}$, is chosen to be 0.01, as in Yuan and Friedmann (1995). Additionally, the constraints are modified for the 2nd lag mode, which can sometimes be slightly unstable. To prevent this situation, a small amount of structural damping is added to this mode, as in Yuan and Friedmann (1998). For this study, 0.5% structural damping is added to stabilize the 2nd lag mode of the baseline blade. For the yielding constraint, a factor of safety of 1.5 is used. The rotor blade was discretized into the 6 finite elements shown in Fig. 7.

5.1 Practical implementation details associated with the surrogates

Four approximation methods were compared: 2nd order polynomials, RBF interpolation, ordinary kriging, and kriging where all p_k are not fixed at 2. The surrogates were fit to the sample data using MATLAB programs on a 3.2 GHz Xeon processor. In this study, the ordinary kriging surrogates were created with a freely available MATLAB kriging toolbox (Lophaven et al 2002). In the parameter estimation, a local optima of the likelihood function (19) is sought. Since this algorithm is only configured for ordinary kriging, a different MATLAB package is used for the more general kriging. The MATLAB package used for the more general kriging utilizes the global search algorithm DIRECT (Sasena 2002; Jones 2001) for optimization of the likelihood function. Since the DIRECT algorithm results in a more global optimization, the more general kriging algorithm is not as efficient as the ordinary kriging algorithm.

In this study, two sets of fitting points are used to build the surrogates – a 300 point optimal Latin hypercube (OLH) and a 500 point OLH. From the 300 point OLH, 283 points had converged trim solutions and were used to build the surrogates; while out of the 500 point OLH, 484 points had converged trim solutions. The fitting times for each approximation method are given in Table 4. For the kriging surrogates, the majority of the fitting time is devoted to the maximum-likelihood parameter estimation, while for the RBF's, the leave-one-out cross validation method of finding the fitting parameter is responsible for most of the fitting time. The prediction time was much less than one second for each approximation method.

One of the advantages of surrogate based optimization with design of computer experiments is that each simulation corresponding to a design point in the OLH can be run independently of the other design points, and therefore the simulations can be run in parallel. The helicopter simulations were run on a Linux cluster with 1.8 Ghz Opteron processors. The simulation time was about 6 hours per simulation and 20 to 60 simulations were run simultaneously.

Table 3 Upper and lower bounds on the fundamental frequencies (/rev)

	Flap	Lag	Torsion
ω_U	1.20	0.80	6.50
ω_L	1.05	0.60	2.50

Table 4 Fitting times associated with the approximation methods on a 3.2 GHz Xeon processor

Surrogate	Sample Size	Fitting Time
Poly.	283	< 1 s
RBF	283	1.5 - 2 min.
Ord. krg.	283	15 - 20 s
Krg.	283	4 - 5 min.
Poly.	484	< 1 s
RBF	484	8 - 9 min.
Ord. krg.	484	50 s - 1 min.
Krg.	484	14 - 15 min.

5.2 Surrogate accuracy results

The predictive capabilities of the approximation methods discussed in Section 4 were compared using the two sets of fitting points. In order to quantify the accuracy of the surrogates, two methods for calculating error were considered. The first method requires conducting additional simulations at test points which are independent of the fitting points, in order to test the predictions of the surrogates. The second method is based on leave-one-out cross validation and seeks to represent the error in the surrogate without conducting additional expensive simulations.

5.2.1 Errors based on additional test points

The first method for quantifying the error in the surrogates utilizes simulation data at test points which are not included in the optimal Latin hypercubes used to create the surrogates. The predicted responses from the surrogates were then compared to the "actual" responses at the test points. The test points came from a 200 point OLH, of which 197 had converged trim solutions. None of the blade designs from the 197 test points were coincident with the blade designs from the two OLH's used to create the surrogates. Using the test points, the absolute percent error is given by

$$\varepsilon_i^{(tp)} = \frac{|y^{(i)} - \hat{y}^{(i)}|}{\bar{y}} \tag{32}$$

where $y^{(i)}$ is the "actual" response computed by the helicopter simulation, $\hat{y}^{(i)}$ is the response predicted by the surrogate at the i^{th} test point, and $\bar{y}$ is the mean of the absolute values of the responses from the 197 test points. Based on (32), the average percent error, maximum percent error, and minimum percent error are:

$$\varepsilon_{avg}^{(tp)} = \frac{\sum_{i=1}^{N_{tp}} \varepsilon_i^{(tp)}}{N_{tp}} \tag{33}$$

$$\varepsilon_{max}^{(tp)} = \text{Max}\left\{\varepsilon_1^{(tp)}, \ldots, \varepsilon_{N_{tp}}^{(tp)}\right\} \tag{34}$$

$$\varepsilon_{min}^{(tp)} = \text{Min}\left\{\varepsilon_1^{(tp)}, \ldots, \varepsilon_{N_{tp}}^{(tp)}\right\} \tag{35}$$

where N_{tp} is the number of test points. The minimum and maximum percent errors represent the best and worst predictive errors respectively. These error measures are localized since they only represent one point of the 197 test points, while the average percent error represents the surrogate's predictive capability over the entire design space since all 197 test points are included.

The average and maximum percent errors in the approximations of the hub shears and moments are given in Figs. 8 and 9 respectively. The minimum errors are very low – under 1% for each approximation method – and are not shown for the sake of brevity. Figure 8 shows that one of the kriging surrogates was the most accurate for every shear and moment in terms of average error, while the polynomial response surface generally had the highest average errors. Typically, the more general kriging surrogate had the lowest average errors, which ranged from 11-51% with 283 sample points and 11-42% with 484 sample points. Figure 8 shows that the kriging models are superior in terms of accurately modeling the hub shears

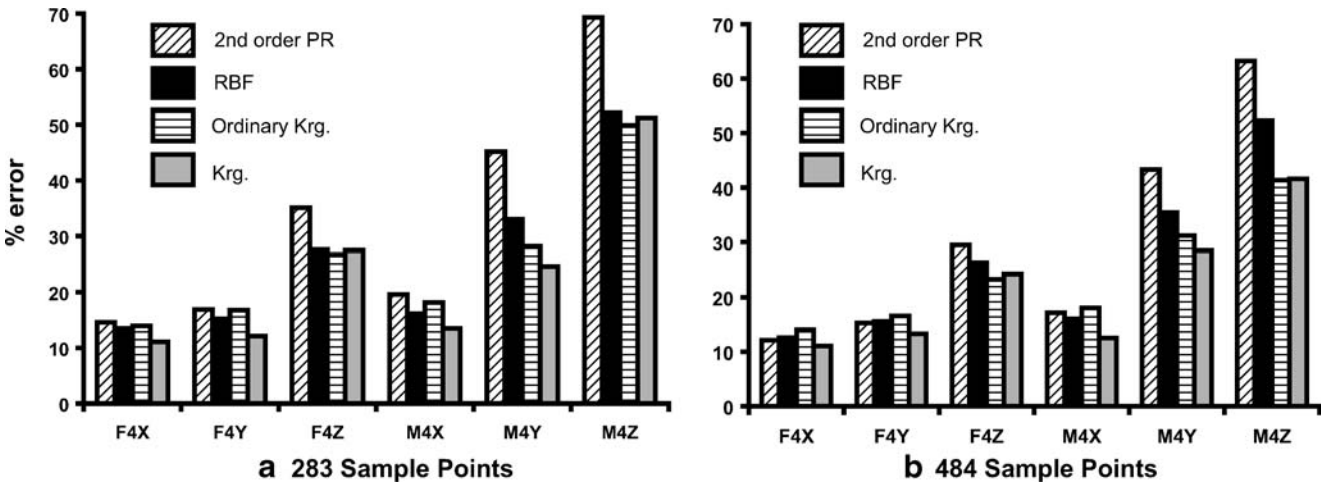

Fig. 8 Average errors of the underlying vibratory loads, relative to mean responses

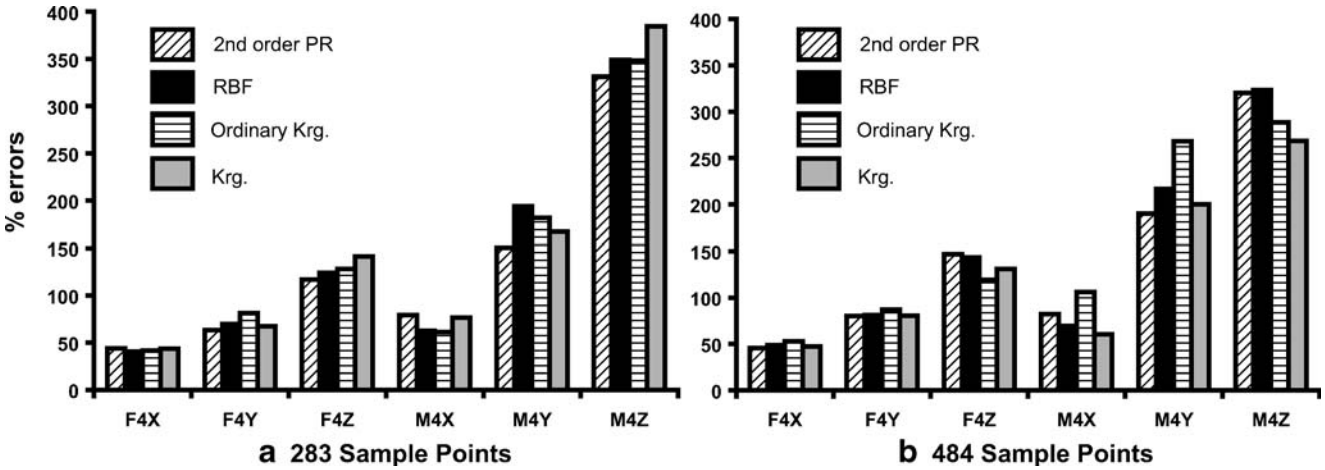

Fig. 9 Maximum errors of the underlying vibratory loads, relative to mean responses

and moments over the entire designs space, and that the kriging model which includes p_k in the maximum likelihood estimation generally outperformed the ordinary kriging model. Even though the more general kriging model typically has lower average errors than ordinary kriging, the differences are not large. The largest difference in error between the two kriging models was only 5.5%, which occurred in the case of the M_{4X} surrogate based on 484 sample points. A comparison of the final fitting parameters of both kriging models is given in Appendix B.

With the exception of the polynomial response surfaces, increasing the number of sample points did not always reduce the average errors in the approximate vibratory loads. In fact, for some surrogate vibratory loads, *higher* average errors were associated with the 484 sample set. The most drastic case is associated with the M_{4Y} surrogate in which the error for the more general kriging surrogate was 3.9% higher when using 484 sample points as opposed to 283. These results indicate that for the 17 dimensional design space, increasing the number of fitting points from 283 to 484 was not sufficient to significantly enhance the accuracy of the surrogates over the entire design space.

Figure 9 shows that all of the approximation methods are susceptible to high maximum errors, which range from 40-385% for 283 sample points, and 46-324% for 484 sample points. These results suggest that there are local regions in the design space where the surrogates are not reliable. Furthermore, increasing the number of sample points did not always reduce the maximum error, just as with average error.

The average and maximum errors in the surrogate objective function are given in Figs. 10 and 11. The surrogate objective functions were generated by two approaches: (a) combining the surrogate hub shears and moments to form the approximate objective function as in (10) and (b) by directly fitting the outputs for J at the sample points. Figure 10 shows that constructing the surrogates from the approximate underlying responses results in slightly lower average errors for both sample sizes. The largest difference in average

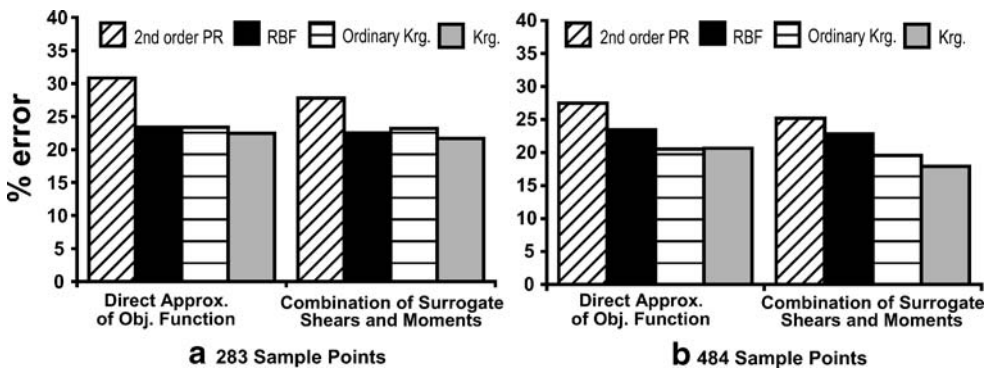

Fig. 10 Average errors in the surrogate objective function, relative to mean responses

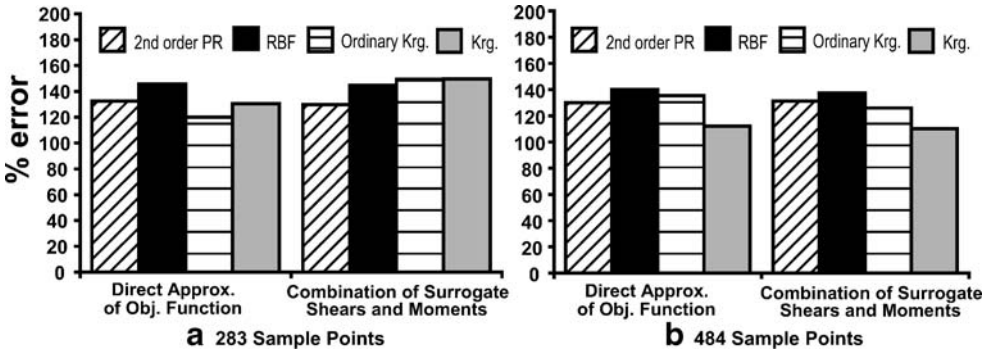

Fig. 11 Maximum errors in the surrogate objective function, relative to mean responses

error between the two methods for creating the surrogate objective function was only 3.2% and occurred when using polynomials with 283 sample points.

Figure 11 shows that both methods of approximating the vibration objective function result in maximum errors above 100%, and thus both methods are susceptible to very high errors in local regions of the design space. However, in contrast to the results in Fig. 10 for average error, generating the surrogate objective function from the underlying vibratory hub loads did not always result in lower maximum errors. So approximating the underlying responses offered a small advantage for modeling the objective function over the entire design space, but neither method offered a clear advantage in terms of maximum error.

The errors in the approximate yielding constraint (9) are given in Figs. 12 a,b. The ordinary kriging surrogate best approximates the constraint over the entire design space, with average errors of 35% using 283 sample points and 31% using 484 sample points. There are large maximum errors (over 300%) with all the approximation methods, thus the surrogate constraints may not be reliable in certain regions of the design space. The more general kriging surrogate has the highest average and maximum errors when using 484 sample points. This is because during the maximum-likelihood estimation of the fitting parameters, the correlation matrix (15) became ill-conditioned, which is not unheard of (Martin and Simpson 2005), so the auxiliary optimization process used to find the fitting parameters did not progress to completion.

5.2.2 Errors based on leave-one-out cross validation

The second method for quantifying the error is based on leave-one-out cross validation. In this approach, error is calculated as follows:

1. A single design point is removed from the OLH data used to fit the surrogate.
2. The surrogate is created using the remaining $(N_{sp}-1)$ sample points.
3. The surrogate is evaluated at the left out design and compared to the actual response.

Thus, the cross validation error is given by

$$\varepsilon_i^{(cv)} = \frac{|y^{(i)} - \hat{y}^{(-i)}|}{\bar{y}} \tag{36}$$

where $\hat{y}^{(-i)}$ is the surrogate's prediction at the left out sample point when the surrogate is fit to the $(N_{sp}-1)$ remaining points. The average, maximum, and

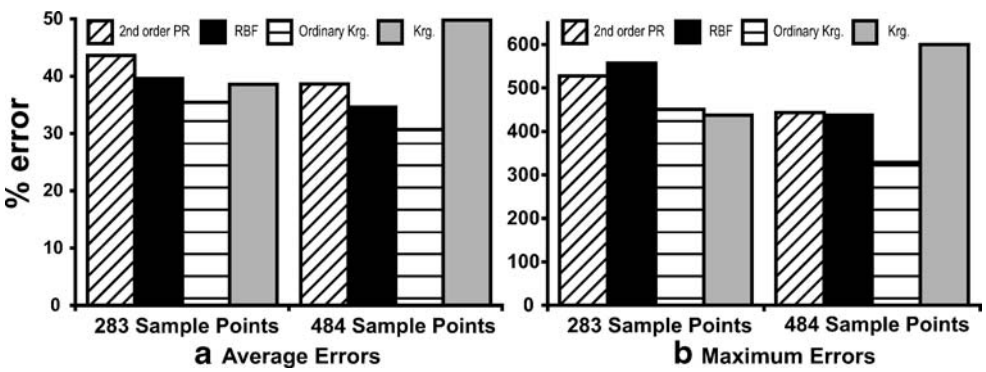

Fig. 12 Errors in the surrogate yielding constraint, relative to mean responses

Table 5 Ratio of average leave-one-out cross validation errors to average errors based on test points

Surrogate	Sample Size	F_{4X}	F_{4Y}	F_{4Z}	M_{4X}	M_{4Y}	M_{4Z}	J	Yielding Constraint
Poly.	283	1.12	1.20	1.19	1.07	1.24	1.25	1.18	1.20
RBF	283	1.01	1.13	0.98	1.06	1.15	1.01	1.00	1.01
Ord. krg.	283	1.10	1.08	1.18	1.01	1.15	1.06	1.09	1.01
Krg.	283	1.06	1.16	0.96	1.15	1.40	1.01	1.05	1.00
Poly.	484	1.18	1.01	1.01	1.14	1.06	1.04	0.96	1.00
RBF	484	1.15	1.02	0.98	1.11	1.11	0.99	0.94	1.04
Ord. krg.	484	1.04	1.04	1.11	1.03	1.22	1.12	1.02	1.13
Krg.	484	1.07	0.98	1.06	1.31	1.15	1.12	1.04	0.96

minimum leave-one-out cross validation errors can be written as:

$$\varepsilon_{avg}^{(cv)} = \frac{\sum_{i=1}^{N_{sp}} \varepsilon_i^{(cv)}}{N_{sp}} \tag{37}$$

$$\varepsilon_{max}^{(cv)} = \text{Max}\left\{\varepsilon_1^{(cv)}, \ldots, \varepsilon_{N_{sp}}^{(cv)}\right\} \tag{38}$$

$$\varepsilon_{min}^{(cv)} = \text{Min}\left\{\varepsilon_1^{(cv)}, \ldots, \varepsilon_{N_{sp}}^{(cv)}\right\} \tag{39}$$

The advantage of using leave-one-out cross validation is that a measure of the error can be obtained using only the simulated data used to create the surrogates, as opposed to conducting expensive simulations at additional test points which are only used to quantify error. However, leave-one-out cross validation errors represent the sensitivity of the surrogate to the left out designs, and may not adequately represent the error in the surrogate. Therefore, the purpose of comparing leave-one-out cross validation error with error based on additional test points is to determine whether the magnitude of error can be predicted without using additional test points. Note that the cross validation error in (36) is normalized by the mean responses from the 197 test points as in (32) so that errors based on (32) and (36) can be directly compared.

The ratio of the leave-one-out cross validation errors to the errors based on test points are given in Tables 5 and 6 for the 6 surrogate hub shears and moments, the directly approximated objective function, and the surrogate yielding constraint. Table 5 shows that the magnitude of the average error can be captured using leave-one-out cross validation, with the largest difference occurring for the M_{4Y} kriging surrogate with 283 sample points where the cross validation error was 1.4 times larger than the error based on test points. Furthermore, the average cross validation error generally gave a more conservative (i.e. a ratio > 1.0) estimate of the error over the entire design space.

Table 6 shows that leave-one-out cross validation also captured the magnitude of the maximum error, with the largest difference corresponding to the M_{4X} kriging surrogate with 484 sample points where the cross validation error was 3.22 times higher than the error based on test points. The maximum leave-one-out cross validation error was typically more conservative for the vibratory surrogates, but tended to underpredict the error in the yielding constraint for the 484 point surrogates. So for the yielding surrogate, whether or not the maximum cross validation error was a conservative measure of error was dependent on the number of sample points used to create the surrogate.

5.3 Robustness

In addition to the accuracy, another metric for quantifying the effectiveness of the surrogates is robustness,

Table 6 Ratio of maximum leave-one-out cross validation errors to maximum errors based on test points

Surrogate	Sample Size	F_{4X}	F_{4Y}	F_{4Z}	M_{4X}	M_{4Y}	M_{4Z}	J	Yielding Constraint
Poly.	283	1.38	1.47	1.84	1.08	1.74	1.11	1.31	1.10
RBF	283	1.29	1.21	1.55	1.45	1.33	1.08	1.25	1.08
Ord. krg.	283	1.18	1.08	1.31	1.75	1.38	1.05	1.35	1.26
Krg.	283	1.14	1.21	1.29	1.31	1.56	1.02	1.44	1.46
Poly.	484	1.04	0.90	1.02	1.33	0.89	1.03	0.94	0.60
RBF	484	1.35	1.08	1.04	3.07	1.36	1.28	1.23	0.68
Ord. krg.	484	1.07	1.08	1.16	1.62	1.33	1.41	1.37	0.76
Krg.	484	1.29	1.17	1.17	3.22	1.45	1.65	1.53	0.79

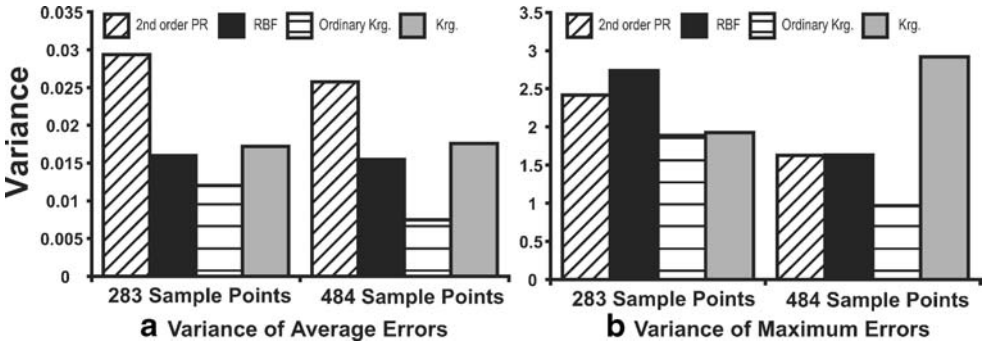

Fig. 13 Variance of the average and maximum error measures (based on test points)

i.e. the capability of the approximation methods to accurately model different responses. The robustness measure indicates how sensitive the performance of an approximation method is to the type of response being modeled. The variance of the average and maximum error measures based on test points is used to quantify robustness (Jin et al 2001). The lower the variance, the more robust the approximation method. Figure 13 gives the variance of the errors for the 8 responses considered in this study: the 6 hub shears and moments, the overall objective function, and the yielding constraint. Ordinary kriging is the most robust approximation method, and thus its performance fluctuates the least when modeling the responses in this study. Furthermore, the variance of each surrogate method, except the more general kriging, is lowered by increasing the number of sample points from 283 to 484. Therefore, for the responses considered in this study, increasing the number of sample points increases the robustness of the surrogates. This conclusion does not hold for the more general kriging due to the ill-conditioned correlation matrix encountered when approximating the yielding constraint.

5.4 Optimization results

The surrogate based optimization (SBO) conducted in this study is *non-updating*, otherwise known as the "one-shot" approach, which means that the surrogate is not updated with objective function evaluations as the optimization progresses. While it is important to use an updating method so that optimization does not lead to regions of high uncertainty in the surrogate, the focus of this study was on the effectiveness of the approximation techniques and not on the search algorithm. Optimization of the surrogate objective functions was conducted with the Multi-Island Genetic Algorithm in iSIGHT. Each of the approximation methods was used to generate the surrogate yielding constraint. However, changing the type of approximation method used to create the surrogate constraint did not alter the optimal design. Although the type of approximation method used to model the yielding constraint did not make a difference, it was necessary to include the surrogate yielding constraint since optimizing without it led to designs which yield at the root. Helicopter simulations were conducted at the optimal designs to obtain the "actual" amount of vibration reduction.

Table 7 gives the optimization results when using the underlying hub shears and moments to build the surrogate objective function. Note that vibration reduction is computed relative to the vibration levels of a baseline blade resembling an MBB BO-105 blade. Table 7 shows that all approximation methods lead to significant vibration reduction of over 50% and ordinary kriging leads to the best designs, with vibration reduction of 67.4% with 283 sample points and 66.1% with 484 sample points.

Table 7 Comparison of predicted and "actual" vibration reductions using approximate underlying responses, relative to MBB B0-105 baseline values

Surrogate	Sample Size	Predicted Reduction	Actual Reduction	ω_{L1}	ω_{F1}	ω_{T1}
Poly.	283	100.0 %	66.4 %	0.671	1.062	5.036
RBF	283	100.0 %	55.2 %	0.605	1.064	3.783
Ord. krg.	283	92.6 %	67.4 %	0.611	1.060	4.583
Krg.	283	95.3 %	51.0 %	0.617	1.064	4.136
Poly.	484	100.0 %	58.9 %	0.608	1.056	3.958
RBF	484	100.0 %	57.7 %	0.600	1.059	4.165
Ord. krg.	484	94.9 %	66.1 %	0.616	1.061	4.483
Krg.	484	94.2 %	64.5 %	0.624	1.063	4.383

Table 8 Comparison of predicted and "actual" vibration reductions when directly approximating the objective function, relative to MBB B0-105 baseline values

Surrogate	Sample Size	Predicted Reduction	Actual Reduction	ω_{L1}	ω_{F1}	ω_{T1}
Poly.	283	394.4 %	64.4 %	0.610	1.058	4.330
RBF	283	132.8 %	51.9 %	0.600	1.060	4.054
Ord. krg.	283	144.4 %	63.8 %	0.615	1.061	4.404
Krg.	283	105.6 %	52.8 %	0.602	1.060	4.314
Poly.	484	222.4 %	45.0 %	0.627	1.060	3.960
RBF	484	136.4 %	52.2 %	0.602	1.061	3.958
Ord. krg.	484	162.8 %	54.7 %	0.613	1.061	4.283
Krg.	484	124.0 %	53.2 %	0.600	1.060	4.234

Table 8 shows that significant vibration reduction can also be achieved when directly approximating the objective function, however the amount of reduction was generally less than the results in Table 7. This is because by approximating the underlying responses, the behavior of the vertical shear F_{4Z} is captured, which is important since much of the reduction in the objective function is due to reduction of the vertical shear. The importance of approximating the vertical shear is illustrated in Fig. 14, in which the optimal vibratory loads from ordinary kriging surrogates using 283 sample points are shown with the MBB BO-105 baseline values. Figure 14 shows that approximating the underlying responses leads to 77% reduction of F_{4Z}, while approximating the overall objective function results in 67% reduction of the vertical shear. It is also clear from Fig. 14 that approximating the underlying responses results in higher values for the five other shears and moments compared to direct approximation of the objective function. Thus, approximating the underlying responses led to a superior design because capturing the behavior of the individual shears and moments leads to a more effective reduction of the vertical shear F_{4Z}.

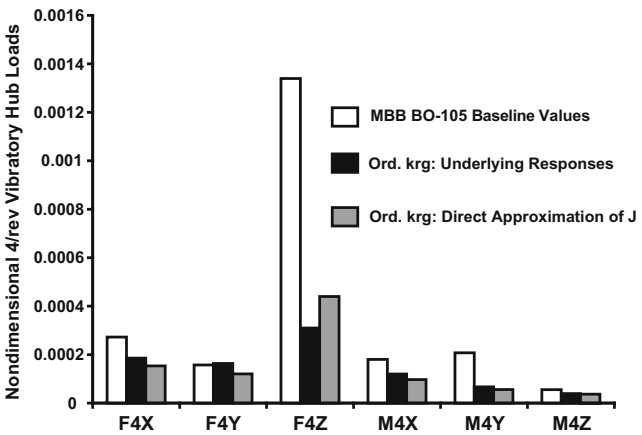

Fig. 14 Comparison of the optimal vibratory loads when using surrogate underlying responses and when directly approximating the objective function

Tables 7 and 8 also show that increasing the number of fitting points did not always improve the optimal designs, and in some instances resulted in worse designs. This is probably due to the 283 sample set having a best feasible design with 52% vibration reduction, which was better than the 48% reduction associated with the best feasible design in the 484 data set. The polynomial surrogates were the most adversely affected by increasing the number of sample points. Furthermore, optimizing the surrogate did not always lead to a better design than the best design in the set of fitting points used to create the surrogates. This occurs because all of the surrogates are inaccurate at the optimal designs. For instance, Table 7 shows that optimizing the more general kriging surrogate based on 283 sample points led to 51% actual reduction, while the surrogate predicts 95.3% reduction. The discrepancy between the predicted reduction and the actual reduction shows that the surrogate is not accurate at the optimal design. Moreover, the optimal design is worse than the best feasible design from the OLH, which produced 52% reduction. So optimizing the surrogate led to a region of the design space where the surrogate was not accurate, and the optimal design happened to be worse than the best feasible design from the fitting data. Although none of the surrogates accurately predict the amount of vibration reduction at the optimal designs, optimizing the surrogates generally led to superior designs than the best feasible designs in the optimal Latin hypercubes.

The fundamental rotating frequencies corresponding to the optimal designs are also given in Tables 7 and 8. No two optimal blade designs have the same set of fundamental frequencies, which means that each surrogate led to a different optimal blade design. These results suggest that, at the flight condition characterized by BVI induced vibrations, there are many local optima in the design space. Table 9 gives the predicted vibration reduction from each surrogate at all of the optimal designs from Table 7. The results from Table 9 show that every surrogate is able to predict that the optimal

Table 9 Predicted vibration reduction by each of the surrogates at all of the optimal designs from Table 7

Optimum	Sample Size	Predicted Reduction by Poly.	Predicted Reduction by RBF	Predicted Reduction by Ord. krg.	Predicted Reduction by Krg.
Poly.	283	100.0 %	83.3 %	15.5 %	95.2 %
RBF	283	69.3 %	100.0 %	24.4 %	72.7 %
Ord. krg.	283	21.5 %	40.9 %	92.6 %	70.7 %
Krg.	283	93.2 %	83.7 %	71.6 %	95.3 %
Poly.	484	100.0 %	84.1 %	61.3 %	74.5 %
RBF	484	63.2 %	100.0 %	34.1 %	58.0 %
Ord. krg.	484	74.1 %	62.7 %	94.9 %	72.5 %
Krg.	484	33.8 %	89.6 %	38.6 %	94.2 %

designs are reduced vibration designs. Therefore, all of the surrogates are able to capture the fact that the objective function has many local optima, which would be important if it were desirable to obtain many prospective optimum designs in addition to the global optimum.

The optimal designs were checked for robustness to small perturbations by perturbing each design variable by $\pm 3\%$ from the optimum value, as in Murugan and Ganguli (2005). None of the perturbed designs resulted in more than 5% difference from the original objective function value, and there was an average change in objective function values of only 1.2% over all the perturbed designs. So the optimal designs were robust to small perturbations in the designs, which indicates that the regions around the optimal designs are reliable regions of reduced vibration designs.

6 Conclusions

The results in this paper demonstrate that global approximation methods, such as polynomial regression, radial basis function interpolation, and kriging, can lead to blade designs with significantly reduced vibration levels. Even with local regions in the design space where the surrogates' predictions are unreliable, the surrogates still captured enough of the behavior over the entire design space such that they could be used to find regions of improved design. Overall, ordinary kriging performed the best in terms of accuracy over the entire design space, robustness, and optimization. The principal results from this study are summarized below.

1. Among the methods considered, kriging was the most effective method for approximating vibratory loads over the entire design space, and for locating an optimum blade design. Although the average accuracies of kriging were the best, the kriging surrogates were susceptible to high errors at certain design points.
2. The high maximum errors suggest that none of the approximation methods can be used for precise predictions of vibrations everywhere in the design space, at least without adding more interpolation points, although they are still useful in finding more optimal designs.
3. Allowing the parameters p_k to vary in the kriging fitting process resulted in surrogates which were generally more accurate over the entire design space, but resulted in inferior blade designs compared to ordinary kriging when used in optimization.
4. Approximating the underlying responses of the objective function, as opposed to directly approximating the objective function, resulted in superior blade designs because of the importance of reducing the vertical shear, F_{4Z}.
5. Ordinary kriging was the most robust of the approximation methods, and therefore the performance of ordinary kriging was the least dependent on the behavior of the response being approximated.
6. By using leave-one-out cross validation, the magnitude of the error in the surrogates can be predicted without generating additional test points. Furthermore, leave-one-out cross validation generally gave a conservative estimate of the error over the entire design space.
7. While all of the approximation methods considered led to significant vibration reduction, ordinary kriging produced the best blade design which had vibration levels 67% less than an MBB BO-105 baseline blade.

Acknowledgements This research was supported in part by the FXB Center for Rotary and Fixed Wing Air Vehicle Design, ARO grant 02-1-0202 with Dr. B. LaMattina as grant monitor, and a NASA GSRP grant for Bryan Glaz. The authors are grateful to Professor R. Haftka for his valuable advice, and Professor P. Papalambros and Dr. S. Gunawan for providing a kriging computer algorithm which was used in this study.

Table 10 Fitting parameters for the ordinary kriging surrogates (283 sample points)

Parameter	F_{4X}	F_{4Y}	F_{4Z}	M_{4X}	M_{4Y}	M_{4Z}	J	Yielding Constraint
ϑ_1	0.354	0.354	0.300	0.354	0.317	0.329	0.317	0.057
ϑ_2	0.258	0.258	0.216	0.258	0.235	0.235	0.219	0.030
ϑ_3	0.188	0.188	0.087	0.188	0.175	0.175	0.151	0.028
ϑ_4	0.137	0.137	0.130	0.177	0.139	0.130	0.112	0.028
ϑ_5	0.100	0.100	0.145	0.100	0.096	0.096	0.078	0.009
ϑ_6	0.073	0.073	0.035	0.073	0.072	0.072	0.055	0.020
ϑ_7	0.079	0.079	0.100	0.079	0.549	0.059	0.122	0.018
ϑ_8	0.039	0.039	0.030	0.039	0.039	0.044	0.099	0.017
ϑ_9	0.028	0.028	0.060	0.028	0.029	0.033	0.039	0.015
ϑ_{10}	0.035	0.024	0.232	0.035	0.556	0.540	0.065	0.100
ϑ_{11}	0.015	0.015	0.011	0.015	0.016	0.019	0.010	0.019
ϑ_{12}	0.011	0.011	0.187	0.011	0.012	0.534	0.042	0.013
ϑ_{13}	0.016	0.016	0.259	0.016	0.531	0.010	0.034	0.100
ϑ_{14}	0.010	0.010	0.030	0.013	0.010	0.011	0.019	0.028
ϑ_{15}	0.010	0.010	0.060	0.010	0.010	0.010	0.019	0.009
ϑ_{16}	0.010	0.010	0.019	0.012	0.010	0.010	0.019	0.016
ϑ_{17}	0.010	0.010	0.013	0.010	0.036	0.036	0.011	0.094

Appendix A: Hover stability perturbation analysis with RFA aerodynamics

The development of the perturbation equations used in the linearized stability analysis are given in this appendix. The process used in Yuan and Friedmann (1995) has been modified to take into account the RFA aerodynamic model. In Yuan and Friedmann (1995), the blade equations of motion were only a function of the blade response and trim parameters, i.e.,

$$\mathbf{f}_b\left(\mathbf{q}_b, \dot{\mathbf{q}}_b, \ddot{\mathbf{q}}_b, \mathbf{q_t}\right) = \mathbf{0} \tag{40}$$

where $\mathbf{q}_b$ is the vector of generalized modal coordinates representing the blade degrees of freedom and $\mathbf{q}_t$ is the vector of trim parameters which are uniform inflow and collective pitch for hover. In this study, the blade equations of motion are written as

$$\mathbf{f}_b\left(\mathbf{q}_b, \dot{\mathbf{q}}_b, \ddot{\mathbf{q}}_b, \mathbf{x}_a, \mathbf{q}_t\right) = \mathbf{0} \tag{41}$$

where $\mathbf{x}_a$ is the vector of aerodynamic states introduced by the RFA aerodynamic model. Correspondingly, there is a set of governing ODE's for the aerodynamic state vector,

$$\dot{\mathbf{x}}_a = \mathbf{g}_a(\mathbf{q}_b, \dot{\mathbf{q}}_b, \ddot{\mathbf{q}}_b, \mathbf{x}_a, \mathbf{q_t}). \tag{42}$$

Table 11 Fitting parameters for the ordinary kriging surrogates (484 sample points)

Parameter	F_{4X}	F_{4Y}	F_{4Z}	M_{4X}	M_{4Y}	M_{4Z}	J	Yielding Constraint
ϑ_1	0.354	0.354	0.289	0.354	0.317	0.538	0.289	0.056
ϑ_2	0.258	0.258	0.216	0.258	0.235	0.187	0.216	0.025
ϑ_3	0.188	0.188	0.161	0.188	0.175	0.134	0.161	0.022
ϑ_4	0.137	0.137	0.121	0.172	0.139	0.161	0.121	0.035
ϑ_5	0.100	0.100	0.090	0.100	0.096	0.070	0.090	0.025
ϑ_6	0.073	0.073	0.067	0.073	0.072	0.050	0.067	0.017
ϑ_7	0.079	0.079	0.097	0.079	0.059	0.075	0.201	0.022
ϑ_8	0.039	0.039	0.078	0.039	0.044	0.112	0.121	0.016
ϑ_9	0.028	0.028	0.028	0.046	0.029	0.045	0.028	0.005
ϑ_{10}	0.035	0.035	0.250	0.035	0.540	1.000	0.269	0.084
ϑ_{11}	0.015	0.015	0.016	0.015	0.016	0.010	0.016	0.011
ϑ_{12}	0.011	0.011	0.032	0.011	0.014	0.161	0.032	0.015
ϑ_{13}	0.016	0.016	0.482	0.016	0.531	0.145	0.216	0.100
ϑ_{14}	0.010	0.013	0.072	0.013	0.071	0.014	0.021	0.029
ϑ_{15}	0.010	0.010	0.034	0.010	0.010	0.058	0.031	0.015
ϑ_{16}	0.010	0.010	0.013	0.012	0.010	0.014	0.015	0.007
ϑ_{17}	0.010	0.010	0.040	0.010	0.036	0.030	0.040	0.037

Table 12 Fitting parameters for the more general kriging surrogates (283 sample points)

Parameter	F_{4X}	F_{4Y}	F_{4Z}	M_{4X}	M_{4Y}	M_{4Z}	J	Yielding Constraint
ϑ_1	0.009	0.043	0.890	0.195	0.691	1.899	1.475	0.152
ϑ_2	0.006	0.006	0.006	0.012	0.071	0.026	0.016	0.152
ϑ_3	0.007	0.055	0.152	0.016	0.007	0.071	0.152	0.016
ϑ_4	0.691	1.475	0.152	1.475	2.445	0.251	1.475	0.152
ϑ_5	0.016	0.118	0.417	0.071	0.071	0.324	0.152	0.016
ϑ_6	0.033	0.043	0.006	0.118	0.417	0.071	0.152	0.152
ϑ_7	1.899	3.149	0.417	1.475	4.054	0.324	1.475	0.152
ϑ_8	0.152	0.251	0.055	0.071	0.016	0.152	0.152	0.016
ϑ_9	0.152	0.251	0.152	0.118	0.091	0.152	0.152	0.016
ϑ_{10}	0.152	0.324	1.899	0.324	4.054	1.475	1.475	1.475
ϑ_{11}	0.007	0.006	0.007	0.007	0.007	0.007	0.016	0.152
ϑ_{12}	0.016	0.007	0.324	0.007	0.091	0.324	0.152	0.016
ϑ_{13}	0.691	0.890	1.899	1.146	1.899	0.071	1.475	1.475
ϑ_{14}	0.016	0.055	0.091	0.033	0.152	0.007	0.152	0.152
ϑ_{15}	0.033	0.033	0.251	0.007	0.055	0.152	0.152	0.016
ϑ_{16}	0.016	0.071	0.033	0.152	0.033	0.009	0.016	0.152
ϑ_{17}	0.152	0.152	0.195	0.152	0.417	0.007	0.152	0.152
p_1	1.660	1.953	1.073	1.880	1.953	1.220	1.000	1.000
p_2	0.780	1.953	0.120	0.120	0.927	1.000	1.660	1.660
p_3	1.880	1.880	1.880	0.340	1.440	1.880	1.000	1.000
p_4	1.880	1.953	0.340	1.953	1.880	1.880	1.660	1.000
p_5	1.220	1.000	1.440	1.880	1.220	0.340	1.000	1.000
p_6	0.340	1.953	1.220	1.880	1.953	0.340	1.000	1.000
p_7	1.880	1.880	1.953	1.953	1.953	1.880	1.660	1.660
p_8	1.880	1.953	1.220	1.293	1.880	1.953	1.000	1.660
p_9	1.880	1.733	1.293	1.000	0.633	1.660	1.000	1.000
p_{10}	1.220	1.147	1.000	1.220	1.953	1.440	1.000	1.000
p_{11}	0.120	1.293	1.513	1.220	1.000	1.880	1.660	1.000
p_{12}	1.220	1.953	1.953	1.220	1.880	1.073	1.000	1.000
p_{13}	1.660	1.953	1.293	1.880	1.733	0.340	1.000	1.660
p_{14}	1.880	1.953	1.953	1.880	1.953	0.120	1.000	1.000
p_{15}	0.120	1.220	1.953	1.000	1.880	1.880	1.000	1.000
p_{16}	1.000	0.267	0.780	1.880	1.880	0.120	1.000	1.000
p_{17}	1.953	0.780	1.953	0.120	1.880	1.880	1.660	1.000

Equations 41 and 42 represent the coupled set of ordinary differential equations that govern the rotor blade system. The components of (41) and (42) are formed numerically as part of the helicopter simulation, and detailed equations for the components can be found in Myrtle (1998) and Liu (2005). Since these equations are coupled, the *combined* system must be linearized. The linearization process is now discussed.

Following the development in Myrtle (1998), (41) is rewritten as

$$\mathbf{f}_b = \mathbf{g}_b(\mathbf{q}_b, \dot{\mathbf{q}}_b, \mathbf{x}_a, \mathbf{q}_t) + \mathbf{M}(\mathbf{q}_b, \mathbf{q}_t)\ddot{\mathbf{q}}_b = \mathbf{0} \tag{43}$$

where

$$\mathbf{M} \equiv \frac{\partial \mathbf{f}_b}{\partial \ddot{\mathbf{q}}_b}. \tag{44}$$

Dependence on $\ddot{\mathbf{q}}_b$ in (42) is eliminated by using (43) and (44), yielding

$$\dot{\mathbf{x}}_a = \mathbf{g}_{aR}(\mathbf{q}_b, \dot{\mathbf{q}}_b, \mathbf{x}_a, \mathbf{q}_t). \tag{45}$$

Perturbing (41) about the static equilibrium and neglecting higher order terms gives

$$\left[\frac{\partial \mathbf{f}_b}{\partial \ddot{\mathbf{q}}_b}\right]_{\mathbf{y}_0} \Delta\ddot{\mathbf{q}}_b + \left[\frac{\partial \mathbf{f}_b}{\partial \dot{\mathbf{q}}_b}\right]_{\mathbf{y}_0} \Delta\dot{\mathbf{q}}_b + \left[\frac{\partial \mathbf{f}_b}{\partial \mathbf{q}_b}\right]_{\mathbf{y}_0} \Delta\mathbf{q}_b + \left[\frac{\partial \mathbf{f}_b}{\partial \mathbf{x}_a}\right]_{\mathbf{y}_0} \Delta\mathbf{x}_a = \mathbf{0} \tag{46}$$

where $\mathbf{y}_0$ is the static equilibrium vector and is given by

$$\mathbf{y}_0 = \begin{bmatrix} \mathbf{q}_{b0} \\ \dot{\mathbf{q}}_{b0} \\ \dot{\mathbf{x}}_{a0} \end{bmatrix} \tag{47}$$

Table 13 Fitting parameters for the more general kriging surrogates (484 sample points)

Parameter	F_{4X}	F_{4Y}	F_{4Z}	M_{4X}	M_{4Y}	M_{4Z}	J	Yielding Constraint
ϑ_1	0.016	0.016	0.890	0.537	0.417	4.054	1.475	0.016
ϑ_2	0.016	0.016	0.043	0.043	0.537	0.007	0.016	0.152
ϑ_3	0.152	0.152	0.152	0.033	0.071	0.417	0.016	0.016
ϑ_4	1.475	1.475	0.537	2.445	4.054	0.417	0.152	0.152
ϑ_5	0.152	0.152	0.118	0.071	0.006	0.152	0.152	0.152
ϑ_6	0.152	0.152	0.007	0.043	0.055	0.152	0.152	0.016
ϑ_7	1.475	1.475	0.691	3.149	1.475	0.691	1.475	0.152
ϑ_8	0.152	0.152	0.043	0.118	0.033	0.417	0.152	0.016
ϑ_9	0.152	0.152	0.152	0.324	0.043	0.152	0.152	0.152
ϑ_{10}	0.152	0.152	2.445	1.475	4.054	4.054	1.475	0.152
ϑ_{11}	0.016	0.016	0.118	0.033	0.007	0.071	0.152	0.152
ϑ_{12}	0.016	0.016	0.007	0.071	0.091	0.251	0.152	0.152
ϑ_{13}	0.152	0.152	1.899	0.890	1.475	0.691	1.475	0.016
ϑ_{14}	0.152	0.152	0.417	0.152	0.324	0.016	0.152	0.152
ϑ_{15}	0.016	0.152	0.324	0.026	0.016	0.006	0.152	0.152
ϑ_{16}	0.016	0.016	0.324	0.043	0.091	0.016	0.016	0.152
ϑ_{17}	0.016	0.152	0.152	0.033	0.020	0.043	0.152	0.152
p_1	1.000	1.660	1.440	0.340	1.293	1.807	1.000	1.000
p_2	1.000	0.340	1.953	1.880	1.660	1.953	0.340	1.000
p_3	1.000	1.000	1.807	0.340	0.707	1.880	1.660	1.000
p_4	1.660	1.660	0.560	1.953	1.733	1.953	1.000	1.000
p_5	1.000	1.660	1.660	1.440	1.660	1.880	1.000	1.000
p_6	1.660	1.660	1.880	0.780	0.927	0.120	1.660	1.000
p_7	1.660	1.660	1.293	1.880	1.293	1.953	1.000	1.000
p_8	1.000	1.000	1.733	1.880	1.367	1.880	1.000	1.000
p_9	1.000	1.660	1.953	1.880	1.880	0.340	1.000	1.000
p_{10}	1.000	1.000	1.880	1.733	1.953	1.953	1.000	1.000
p_{11}	1.000	1.660	0.487	1.513	1.880	0.633	1.000	1.000
p_{12}	1.000	1.660	1.880	1.880	1.953	1.293	1.000	1.000
p_{13}	1.660	1.000	1.660	1.953	1.953	1.587	1.660	1.000
p_{14}	1.000	1.000	1.807	0.707	1.000	1.293	1.000	1.000
p_{15}	1.000	1.660	1.880	1.220	1.220	1.440	1.660	1.000
p_{16}	1.660	1.000	0.340	1.880	1.807	1.807	1.000	1.000
p_{17}	1.000	1.000	1.880	1.880	1.880	1.953	1.000	1.000

The "0" subscript denotes static equilibrium solution.

From (43),

$$\left[\frac{\partial \mathbf{f}_b}{\partial \dot{\mathbf{q}}_b}\right]_{\mathbf{y}_0} = \left[\frac{\partial \mathbf{g}_b}{\partial \dot{\mathbf{q}}_b}\right]_{\mathbf{y}_0} \tag{48}$$

$$\left[\frac{\partial \mathbf{f}_b}{\partial \mathbf{q}_b}\right]_{\mathbf{y}_0} = \left[\frac{\partial \mathbf{g}_b}{\partial \mathbf{q}_b}\right]_{\mathbf{y}_0} \tag{49}$$

$$\left[\frac{\partial \mathbf{f}_b}{\partial \mathbf{x}_a}\right]_{\mathbf{y}_0} = \left[\frac{\partial \mathbf{g}_b}{\partial \mathbf{x}_a}\right]_{\mathbf{y}_0}. \tag{50}$$

Substituting (48)–(50) and (44) into (46) gives

$$[\mathbf{M}]_{\mathbf{y}_0}\,\Delta\ddot{\mathbf{q}}_b + \left[\frac{\partial \mathbf{g}_b}{\partial \dot{\mathbf{q}}_b}\right]_{\mathbf{y}_0}\Delta\dot{\mathbf{q}}_b + \left[\frac{\partial \mathbf{g}_b}{\partial \mathbf{q}_b}\right]_{\mathbf{y}_0}\Delta\mathbf{q}_b + \left[\frac{\partial \mathbf{g}_b}{\partial \mathbf{x}_a}\right]_{\mathbf{y}_0}\Delta\mathbf{x}_a = \mathbf{0} \tag{51}$$

Solving for $\Delta\ddot{\mathbf{q}}_b$ yields

$$\Delta\ddot{\mathbf{q}}_b = -\mathbf{M}^{-1}\left[\frac{\partial \mathbf{g}_b}{\partial \dot{\mathbf{q}}_b}\right]_{\mathbf{y}_0}\Delta\dot{\mathbf{q}}_b - \mathbf{M}^{-1}\left[\frac{\partial \mathbf{g}_b}{\partial \mathbf{q}_b}\right]_{\mathbf{y}_0}\Delta\mathbf{q}_b - \mathbf{M}^{-1}\left[\frac{\partial \mathbf{g}_b}{\partial \mathbf{x}_a}\right]_{\mathbf{y}_0}\Delta\mathbf{x}_a. \tag{52}$$

Similarly, (45) can be linearized, yielding

$$\Delta\dot{\mathbf{x}}_a = \left[\frac{\partial \mathbf{g}_{aR}}{\partial \dot{\mathbf{q}}_b}\right]_{\mathbf{y}_0}\Delta\dot{\mathbf{q}}_b + \left[\frac{\partial \mathbf{g}_{aR}}{\partial \mathbf{q}_b}\right]_{\mathbf{y}_0}\Delta\mathbf{q}_b + \left[\frac{\partial \mathbf{g}_{aR}}{\partial \mathbf{x}_a}\right]_{\mathbf{y}_0}\Delta\mathbf{x}_a. \tag{53}$$

Combining (52) and (53) with the trivial perturbation equation $\Delta\dot{\mathbf{q}}_b = \Delta\dot{\mathbf{q}}_b$ into first-order state space form gives

$$\dot{\mathbf{z}} = [\mathbf{A}(\mathbf{y}_0)]\mathbf{z} \tag{54}$$

where

$$[\mathbf{A}(\mathbf{y}_0)] = \begin{bmatrix} \mathbf{0} & \mathbf{I} & \mathbf{0} \\ -\mathbf{M}^{-1}\left[\frac{\partial \mathbf{g}_b}{\partial \mathbf{q}_b}\right]_{\mathbf{y}_0} & -\mathbf{M}^{-1}\left[\frac{\partial \mathbf{g}_b}{\partial \dot{\mathbf{q}}_b}\right]_{\mathbf{y}_0} & -\mathbf{M}^{-1}\left[\frac{\partial \mathbf{g}_b}{\partial \mathbf{x}_a}\right]_{\mathbf{y}_0} \\ \left[\frac{\partial \mathbf{g}_{aR}}{\partial \mathbf{q}_b}\right]_{\mathbf{y}_0} & \left[\frac{\partial \mathbf{g}_{aR}}{\partial \dot{\mathbf{q}}_b}\right]_{\mathbf{y}_0} & \left[\frac{\partial \mathbf{g}_{aR}}{\partial \mathbf{x}_a}\right]_{\mathbf{y}_0} \end{bmatrix} \tag{55}$$

and

$$\mathbf{z} \equiv \Delta \mathbf{y} = \begin{bmatrix} \Delta \mathbf{q}_b \\ \Delta \dot{\mathbf{q}}_b \\ \Delta \mathbf{x}_a \end{bmatrix} \tag{56}$$

As mentioned, the stability of the system is determined by the eigenvalues of **A**.

Appendix B: Comparison of Kriging fitting parameters

A comparison of the final fitting parameters for the two kriging models is given in Tables 10, 11, 12, 13. The difference in fitting parameters shows that the two methods of kriging resulted in completely different surrogates.

References

Alexandrov N, Dennis Jr JE, Lewis RM, Torczon V (1998) A trust region framework for managing the use of approximate models in optimization. Struct Optim 15(1):16–23

Booker AJ, Dennis Jr JE, Frank PD, Serafini DB, Torczon V, Trosset MW (1999) A rigorous framework for optimization of expensive functions by surrogates. Struct Optim 17:1–13

Celi R (1999) Recent applications of design optimization to rotorcraft - a survey. J Aircraft 36(1):176–189

Celi R, Friedmann PP (1990) Structural optimization with aeroelastic constraints of rotor blades with straight and swept tips. AIAA J 28(5):928–936

Chen VCP, Tsui K, Barton RB, Meckesheimer M (2006) A review on design, modeling, and applications of computer experiments. IIE Trans 38:273–291

Depailler G, Friedmann PP (2002) Reductions of vibrations due to dynamic stall in helicopters using an actively controlled flap. In: Proceedings of the 43rd AIAA/ASME/ASCE/AHS/ACS Structures, Structural Dynamics and Materials Conference, Denver, CO, AIAA Paper No. 2002-1431

Forsberg J, Nilsson L (2005) On polynomial response surfaces and kriging for use in structural optimization of crashworthiness. Struct Multidisc Optim 29(3):232–243

Friedmann PP (1991) Helicopter vibration reduction using structural optimization with aeroelastic/multidisciplinary constraints - a survey. J Aircr 28(1):8–21

Friedmann PP, Millott T (1995) Vibration reduction in rotorcraft using active control: a comparison of various approaches. J Guidance, Control, Dyn 18(4):664–673

Friedmann PP, Shanthakumaran P (1984) Optimum design of rotor blades for vibration reduction in forward flight. J Am Helicopter Soc 29(4):70–80

Ganguli R (2002) Optimal design of a low vibration helicopter rotor using response surface approximation. J Sound Vib 258(2):327–344

Ganguli R (2004) Survey of recent developments in rotorcraft design optimization. J Aircr 41(3):493–510

Glaz B, Friedmann PP, Liu L (2006) Surrogate based optimization of helicopter rotor blades for vibration reduction in forward flight. In: 47th AIAA/ASME/ASCHE/AHS/ASC Structures, Structural Dynamics & Materials Conference, Newport, RI, pp 1–21, AIAA Paper 2006-1821

Jin R, Chen W, Simpson TW (2001) Comparative studies of metamodeling techniques under multiple modeling criteria. Struct Multidisc Optim. 23:1–13

Jin R, Chen W, Sudjianto A (2005) An efficient algorithm for constructing optimal design of computer experiments. J Stat Plan Inference 134(1):268–287

Johnson W (1988a) CAMRAD/JA - A Comprehensive Analytical Model of Rotorcraft Aerodynamics and Dynamics, Vol I. Theory Manual. Johnson Aeronautics, Palo Alto, CA

Johnson W (1988b) CAMRAD/JA - A Comprehensive Analytical Model of Rotorcraft Aerodynamics and Dynamics, Vol II. Users' Manual. Johnson Aeronautics, Palo Alto, CA

Jones DR (2001) The direct global optimization algorithm. Encyclopedia Optim 1:431–440

Jones DR, Schonlau M, Welch WJ (1998) Efficient global optimization of expensive black-box functions. J Global Optim 13:455–492

Koch PN, Evans JP, Powell D (2002) Interdigitation for effective design space exploration using iSIGHT. Struct Multidisc Optim 23(2):111–126

Lim JW, Chopra I (1989) Aeroelastic optimization of a helicopter rotor. J Am Helicopter Soc 34(1):55–62

Lim JW, Chopra I (1991) Aeroelastic optimization of a helicopter rotor using an efficient sensitivity analysis. J Aircr 28(1):29–37

Liu L (2005) BVI induced vibration and noise alleviation by active and passive approaches. PhD thesis, University of Michigan, Aerospace Engineering

Liu L, Friedmann PP, Patt D (2005) Simultaneous vibration and noise reduction in rotorcraft - practical implementation issues. In: Proceedings of the 46th AIAA/ASME/ASCE/AHS/ACS Structures, Structural Dynamics and Materials Conference, Austin, TX, AIAA Paper 2005-2245

Lophaven SN, Nielsen HB, Søndergaard J (2002) A Matlab Kriging Toolbox, Version 2.0. Informatics and Mathematical Modeling, DTU, Technical Report IMM-TR-2002-12

Martin J, Simpson T (2005) Use of kriging models to approximate deterministic computer models. AIAA J 43(4):853–863

McKay MD, Beckman RJ, Conover WJ (1979) A comparison of three methods for selecting values of input variables in the analysis of output from a computer code. Technometrics 21(2):239–245

Millott TA, Friedmann PP (1994) Vibration Reduction in Helicopter Rotors Using an Actively Controlled Partial Span Trailing Edge Flap Located on the Blade. NASA CR 4611

Murugan S, Ganguli R (2005) Aeroelastic stability enhancement and vibration supression in a composite helicopter rotor. J Aircr 42(4):1013–1024

Myrtle TF (1998) Development of an improved aeroelastic model for the investigation of vibration reduction in helicopter rotors using trailing edge flaps. PhD thesis, University of California, Los Angeles, Mechanical and Aerospace Engineering

Myrtle TF, Friedmann PP (2001) Application of a new compressible time domain aerodynamic model to vibration reduction in helicopters using an actively controlled flap. J Am Helicopter Soc 46(1):32–43

Palmer K, Realff M (2002a) Metamodeling approach to optimization of steady-state flowsheet simulations - model generation. Trans Inst Chem Eng 80(7):760–772

Palmer K, Realff M (2002b) Optimization and validation of steady-state flowsheet simulation metamodels. Trans Inst Chem Eng 80(7):773–782

Patt D, Liu L, Friedmann PP (2005) Rotorcraft vibration reduction and noise prediction using a unified aeroelastic response simulation. J Am Helicopter Soc 50(1):95–106

Patt D, Liu L, Friedmann PP (2006) Simultaneous vibration and noise reduction in rotorcraft using aeroelastic simulation. J Am Helicopter Soc 51(2):127–140

Queipo NV, Haftka RT, Shy W, Goel T, Vaidyanathan R, Tucker PK (2005) Surrogate-based analysis and optimization. Prog Aerospace Sci 41:1–28

Sacks J, Welch WJ, Mitchell TJ, Wynn HP (1989) Design and analysis of computer experiments. Stat Sci 4(4): 409–435

Sasena M (2002) Flexibility and efficiency enhancements for constrained global optimization with kriging approximations. PhD thesis, University of Michigan, Mechanical Engineering

Schmit LA, Miura H (1976) Concepts for Efficient Structural Synthesis. NASA CR-2552

Schonlau M (1997) Computer experiments and global optimization. PhD thesis, University of Waterloo, Statistics and Actuarial Science

Shultz LA, Panda B, Tarzanin FJ, Derham RC, Oh BK, Dadone L (1994) Interdisciplinary analysis for advanced rotors - approach, capabilities, and status. In: American Helicopter Society Aeromechanics Specialists Conference, PS 4-1-4-15

Simpson TW, Mauery TM, Korte JJ, Mistree F (2001a) Kriging models for global approximation in simulation-based multidisciplinary design optimization. AIAA J 39(12):2233–2241

Simpson TW, Peplinski D, Koch PN, Allen JK (2001b) Metamodels for computer-based engineering design: Survey and recommendations. Eng Comp 17:129–150

Simpson TW, Booker AJ, Ghosh D, Giunta AA, Koch PN, Yang R (2004) Approximation methods in multidisciplinary analysis and optimization: A panel discussion. Struct Multidisc Optim 27(5):302–313

Sóbester A, Leary SJ, Keane AJ (2004) A parallel updating scheme for approximating and optimizing high fidelity computer simulations. Struct Multidisc Optim 27:371–383

Stander N, Roux W, Giger M, Redhe M, Fedorova N, Haarhoff J (2004) A comparison of metamodeling techniques for crashworthiness optimization. In: 10th AIAA/ISSMO Multidisciplinary Analysis & Optimization Conference, Albany, New York, pp 1–11, AIAA Paper 2004-4489

de Terlizzi M, Friedmann PP (1998) Aeroelastic response of swept tip rotors including the effects of BVI. In: Proceedings of the 54th Annual Forum of the American Helicopter Society, Washington D.C., pp 644–663

de Terlizzi M, Friedmann PP (1999) Active control of BVI induced vibrations using a refined aerodynamic model and experimental correlation. In: Proceedings of the 55th Annual Forum of the American Helicopter Society, Montreal, Canada, pp 599–615

Won K, Ray T (2005) A framework for design optimization using surrogates. Eng Optim 37(7):685–703

Wujek BA, Renaud JE (1998) Improved trust region model management for approximate optimization. In: Advances in Design Automation, Atlanta, Georgia, paper No. DETC98/DAC-5616

Yuan KA, Friedmann PP (1995) Aeroelasticity and Structural Optimization of Composite Helicopter Rotor Blades with Swept Tips. NASA CR 4665

Yuan KA, Friedmann PP (1998) Structural optimization for vibratory loads reduction of composite helicopter rotor blades with advanced geometry tips. J Am Helicopter Soc 43(3):246–256